Mesoscale Organization and Cloud Microphysics in a Bay of Bengal Depression

ROBERT A. HOUZE, JR. AND DEAN D. CHURCHILL

Department of Atmospheric Sciences, University of Washington, Seattle, WA 98195

(Manuscript received 23 June 1986, in final form 6 January 1987)

ABSTRACT

Airborne radar and cloud microphysical data were obtained throughout a monsoon depression observed over the Bay of Bengal on 3–8 July 1979 during the Summer Monsoon Experiment of the Global Atmospheric Research Programme. The precipitation in the disturbance occurred in mesoscale rain areas 100–300 km in horizontal dimension, with the largest areas tending to be elongated in the east–west or northwest–southeast direction. These mesoscale precipitation features resembled the rain areas of equatorial cloud clusters. Each mesoscale precipitation feature contained intense convective cells, but the area covered by rain was predominantly stratiform. The convective cells in the mesoscale features were sometimes arranged in rapidly moving, rather narrow arc-shaped east–west lines, with the stratiform precipitation trailing the line. In other cases, the convective cells were more randomly embedded in the stratiform rain. Ice particle images obtained at flight-level temperatures of +5 to −25°C indicated the precipitation mechanisms in the stratiform regions of the mesoscale precipitation features. Crystals were growing in habits determined by the ambient temperature and were drifting downward. Liquid water was virtually absent above the 0°C level. Pristine shapes, including needles, columns, plates and dendrites were observed in maximum concentration about a kilometer below the altitude where their growth habit was determined. Large dendritic crystals apparently aggregated to form large snowflakes. As ice particles fell below the 0°C level, they abruptly melted to form the drops that constituted the stratiform rain. These observations of precipitation growth and fallout imply that mesoscale updraft motion strong enough to promote ice particle growth, but not strong enough to prevent sedimentation of the particles or to maintain liquid water in the presence of ice, was prevalent at upper levels in the stratiform regions of the mesoscale precipitation features.

1. Introduction

Depressions that form over the Bay of Bengal and move westward over northern and central India are the primary producers of precipitation in that region during the summer monsoon. Although these depressions have been studied extensively [see Ramage (1971) and Rao (1976) for reviews, and Godbole (1977) for a composite analysis of their structure over land], knowledge of the structure and organization of the clouds and rain within them has been greatly limited by the lack of adequate satellite, radar and aircraft observations, especially over the Bay, where the depressions develop. To fill this observational gap, the Summer Monsoon Experiment of the Global Atmospheric Research Programme (Summer MONEX) was organized in 1979 to study, among other things, the nature and characteristics of precipitation in monsoon depressions over the Bay of Bengal.

Summer MONEX achieved the detailed investigation of a depression in the Bay of Bengal on 3–8 July 1979. As part of this investigation, two aircraft were deployed to document the characteristics of the depression. One of these aircraft, the National Oceanic and Atmospheric Administration's WP3D research aircraft (hereafter called the P3), had quantitative radar and cloud microphysical probes aboard. The measurements obtained with these airborne instruments provide an unprecedented view of the structure and organization of the precipitating clouds in the Bay of Bengal depression, and they constitute the set of data upon which the present study is based.

Previous studies of the 3–8 July 1979 Bay of Bengal depression have described its synoptic-scale setting (Krishnamurti et al., 1980; Nitta and Masuda, 1981; Sanders, 1984). In addition, Warner (1984a) and Warner and Grumm (1984) described the flight-level winds and thermodynamic data and the visually observed cloud organization near the core of the depression on 7 July. Warner (1984b) has described some of the cloud structures on 5 July and augmented his analysis with images from the Microwave Sounding Unit (MSU) aboard the TIROS-N satellite. Johnson and Houze (1987) summarize these results and present some preliminary findings from our present analysis.

Although these previous studies note the presence of mesoscale precipitation features associated with the Bay of Bengal depression and describe some of their aspects, there has not been an exhaustive study of the available radar and microphysical data to describe the precipitation patterns and processes in the storm. In our study, we have used the complete set of airborne radar and cloud microphysical data from the P3 to examine both the mesoscale characteristics of the pre-

cipitation areas within the storm and the microstructure of the individual precipitation particles in the clouds associated with the rain areas.

This paper has two objectives:

1) To show that the rain areas in the monsoon depression were similar in scale and organization to mesoscale precipitation areas of cloud clusters in equatorial regions.

2) To determine the vertical distribution of ice particle growth characteristics in the stratiform regions of the rain areas of the monsoon depression.

The first objective is important to achieve because so little was known about the substorm-scale organization of the precipitating clouds in monsoon depressions prior to Summer MONEX. Ramage's (1971) and Rao's (1976) reviews of early work on the southwest monsoon only indicate the tendency of rain to occur throughout the south and west portions of the storm. Although the precipitating clouds in Bay of Bengal depressions are surely tropical, it cannot be assumed a priori that they resemble the precipitating cloud clusters of equatorial regions, e.g., those seen in GATE[1] (Houze and Betts, 1981) and Winter MONEX[2] (Houze et al., 1981b; Churchill and Houze, 1984a; Houze and Churchill, 1984). The precipitating clouds of the monsoon depression, unlike the equatorial cloud clusters seen in GATE and Winter MONEX, were located within a well organized synoptic-scale cyclone. Sanders, studying the same Bay of Bengal depression that we are examining in this paper, concluded, from aircraft and land-based sounding data, that the area-averaged precipitation produced by the monsoon depression could be accounted for by storm-scale ascent associated with large-scale quasi-geostrophic warm advection, and that the role of convection in the depression was primarily to "add detail" on the small temporal and spatial scales. He also noted that the storm exhibited no hurricane-like structure in its patterns of clouds or other parameters.

In view of Sanders results, three possible types of detailed distribution of clouds and precipitation in the depression can be suggested: (i) All the rain is generated in and falls directly from numerous convective towers triggered in the region of storm-scale ascent. (ii) Widespread rain (in which convection may or may not be embedded) is produced directly by the storm-scale ascent. (iii) The rain is distributed within the area of storm-scale ascent in an ensemble of mesoscale precipitation features similar to cloud clusters seen in the intertropical convergence zone. The first suggestion corresponds to assumptions that have been made in parameterizing the effects of clouds in past studies of the dynamics and energetics of monsoon depressions (Krishnamurti et al., 1976; Shukla, 1978). The second suggestion has to be considered in light of Sanders' (1984) results. Examination of the aircraft radar and microphysical data, however, indicates that suggestion (iii) probably conveys the most accurate view of the rainfall in the monsoon depression, and in this paper we provide circumstantial evidence to that effect.

The second objective of this paper, ascertaining the vertical distribution of microphysical processes in the stratiform regions of the cloud-clusterlike rain areas of the monsoon depression, is important because previous direct documentation of the microphysical structure of cloud clusters (see the Winter MONEX studies of Churchill and Houze, 1984a, and Houze and Churchill, 1984) has been limited to a rather narrow altitude range, from which it is difficult to discern particle evolution. The stratiform character of precipitation regions in cloud clusters has heretofore been inferred indirectly from patterns of radar reflectivity. The Summer MONEX flights in the Bay of Bengal depression were made at a wide range of altitudes, with flight-level temperatures ranging from above zero to −23°C. Thus, this storm provided the first opportunity to determine, from the structures of the ice particles themselves, whether they were growing in a stratiform or convective mode in regions of apparently stratiform radar echo. We show that the aircraft data indeed strongly indicate the stratiform character of particle growth in these regions.

2. Data

a. Radar

The P3 flew missions over the Bay of Bengal on 3, 5, 6, 7 and 8 July. This period covered the history of the depression from its formation on the eastern side of the Bay during the 3rd and 4th, to landfall on the east coast of India on the 8th. The P3 was equipped with digitized C-band weather radars in the nose and lower fuselage; however, only the lower fuselage data have been used in this study since the nose radar data were redundant with the lower fuselage observations and the latter has a narrower horizontal beamwidth (1.1°). Its vertical beamwidth is 4.1°, its wavelength is 5.59°, and its peak power is 70 kW. Other characteristics of the lower-fuselage radar are given by Houze et al. (1981a). This same radar was used in the Winter Monsoon Experiment (Winter MONEX) (Houze et al., 1981a,b; Warner, 1982; Churchill and Houze, 1984a,b; Houze and Churchill, 1984; Johnson and Houze, 1987).

Radar reflectivity measurements obtained with the lower fuselage radar were recorded along azimuthal radials separated by 0.5°, in range intervals of 1.45 km. The data on these tapes were first examined subjectively by sequentially displaying plan position in-

[1] Global Atmospheric Research Programme Atlantic Tropical Experiment.

[2] Global Atmospheric Research Programme Winter Monsoon Experiment.

dicator (PPI) plots of the radar reflectivity on a high-resolution color monitor. Areas of stratiform and convective precipitation and areas of sea and land clutter (echoes returned from land or sea surfaces) could be discerned in the resulting imagery. Precipitation echoes could not be distinguished from land clutter, so no further attempt was made to analyze radar echoes located over land. Sea clutter was identifiable as high reflectivity values that appeared in patterns that tended to move with the aircraft. The graphics display indicated the zenith angle of the radar beam, and we noted that when the beam pointed below the horizon, the sea clutter patterns were more pronounced. Also, in regions where the sea surface was observed to be more turbulent, the sea clutter was more prevalent, as the rough seas present more targets perpendicular to the radar beam. For each data tape perused, we noted approximate beam zenith angles below which sea clutter appeared and the range of distances from the aircraft within which sea clutter was apparent. This information gained in previewing the data was used to help remove sea clutter from final analyses of the data, as described below.

Composite Cartesian maps of reflectivity were constructed by transposing the radar data at each recorded azimuth and range (relative to the aircraft) into a Cartesian grid attached to the earth's surface. The reflectivity values were assigned to 2 km × 2 km elements of the grid and averaged to obtain the final composite echo patterns. Since the storm was moving rather slowly (2–3 m s^{-1}), and the composite maps never contained radar data for more than an hour of flight time, we found it unnecessary to account for storm motion in locating observations within the Cartesian grid.

As the Cartesian maps were generated, data recorded at ranges and azimuths noted to be strongly contaminated by sea clutter in our previewing of the data were deleted. This procedure removed the major features of sea clutter. However, a considerable amount of weaker sea clutter patterns remained, and some additional filtering of the data was required. Since the radar completed two 360° horizontal scans every minute while the aircraft traveled at about 10 km min^{-1}, the 2 km square grid elements on the Cartesian map were typically sampled by radar several times. When we averaged the reflectivity values in each element, we found that the sea clutter patterns generally disappeared. This 2 km × 2 km filter provided adequate resolution for our purposes since this paper is largely concerned with distinguishing between convective areas (~10 km) and mesoscale stratiform regions (~100 km) within the precipitation features traversed by the aircraft. Since this filtering has the potential to eliminate small convective cells from the composite, we often reviewed the color graphics to determine if convective cells were present that did not appear in the composite. This reviewal generally gave us confidence that no significant features were overlooked.

b. Microphysical measurements

Cloud liquid water contents were measured aboard the aircraft with a Johnson-Williams hot-wire device. Above the 0°C level, liquid water, as sensed by this instrument, was scarce. Values seldom registered as high as 0.1 g m^{-3}. Consequently, we infer that the cloud regions penetrated by the P3 aircraft at these altitudes were glaciated, or very nearly so. In view of this situation, our microphysical analysis emphasizes the identification and interpretation of the ice particles encountered along the flight tracks of the aircraft.

The P3 was equipped with two Particle Measurement System (PMS) probes (Knollenberg, 1970). The "cloud" probe detected shadowgrams of hydrometeors up to 1.66 mm in diameter, while the "precipitation" probe detected images up to 6 mm in diameter. We have used data from these same instruments to study winter monsoon cloud clusters (Houze et al., 1981a; Churchill and Houze, 1984a,b; Houze and Churchill, 1984). Further details of the operation and characteristics of PMS probes can be found in Cannon (1976) and Heymsfield (1976). The digital data tapes of particle images used in this study were processed at the National Center for Atmospheric Research (NCAR) to flag bad images and produce images on microfilm and microfiche.

The PMS data collected in the Bay of Bengal depression comprised 8.5 h of flight time, during which the images of approximately 5×10^5 individual particles were obtained. Excluded from analysis were some 3 h of particle data collected on 7 July at levels below the melting layer, where no ice particles were observed.

Also excluded from consideration were PMS data obtained in convective regions. As will be seen in section 3, most of the P3's in-cloud flight tracks were in stratiform regions. Too few data were collected in convective regions to constitute a meaningful sample of data for our purposes. A given 1 min period of microphysical data was judged to be convective if the average vertical velocity for that period exceeded 3 m s^{-1} or if any 1-s average vertical velocity during the 1 min period exceeded 5 m s^{-1}. Removal of these time periods rendered the microphysical dataset more representative of stratiform precipitation. The vertical velocity data obtained on board the P3 during Summer MONEX appeared to have a background noise level of magnitude 1–2 m s^{-1}; so vertical velocities of magnitude $\geq$ 3 m s^{-1} were the lowest values that we considered to be a real signal. Although this threshold may not have excluded all the convectively generated particles from our analysis, it does eliminate the most obvious regions of convective activity.

The particle images on microfilm and microfiche for all the nonconvective regions traversed by the aircraft were examined subjectively to determine the presence of identifiable particle types. The frequency of occurrence of each of the identifiable particle types

was tallied for every minute of the dataset. Although the vast majority of the two-dimensional shadowgrams produced by the probe had no identifiable habit, most of the mesoscale precipitation features had some identifiable particles, and some had episodes of large numbers (more than 30 per minute of flight time, or about 1 L^{-1} of air) of clearly identifiable particles. The horizontal and vertical distributions of these identifiable hydrometeors yielded clues about what cloud processes were active within the mesoscale precipitation features of the depression.

The particle images obtained with the PMS probes were examined with 1 min time resolution. The analyst viewing the particle images counted the number of identifiable particle types in each 1 min sample of data. The types of identifiable particles types included *nearly round particles, needles, columns, plates, small dendritic crystals, large dendritic crystals, sideplanes* and *aggregates.* Examples of the images of these particle types are shown in Fig. 1. The first five types were smaller particles identified in data from the cloud probe, which has higher resolution, while the data from the precipitation probe were used to identify the large dendritic crystals and aggregates. Nearly round particles were interpreted to be raindrops at temperatures exceeding 0°C but appeared by their somewhat rough edges to be either graupel or small aggregates at subzero temperatures. Needles were distinguished from columns by their ratio of width to length; columns were defined to have length/width less than about 5, while needles had length/width greater than about 5. These ratios were estimated visually by the analyst. Dendritic crystals exhibited six regularly spaced arms. Occasionally the two-dimensional images of branched crystals exhibited five irregularly spaced arms. This type of image, generally observed at flight-level temperatures below −15°C, is interpreted as a two-dimensional shadow of sideplane crystal (Houze and Churchill, 1984). Dendritic crystals were classified as large if they had a maximum dimension ⩾ 2 mm. Aggregates were considered to be all particles of maximum dimension ⩾ 3 mm, other than those counted as large dendritic crystals. This designation seemed appropriate since the overwhelming majority of images of these large, nondendritic crystals had the highly irregular shape and physical appearance of aggregated ice particles.

In Fig. 1, an icon is indicated to represent each of the identified particle types. In subsequent diagrams,

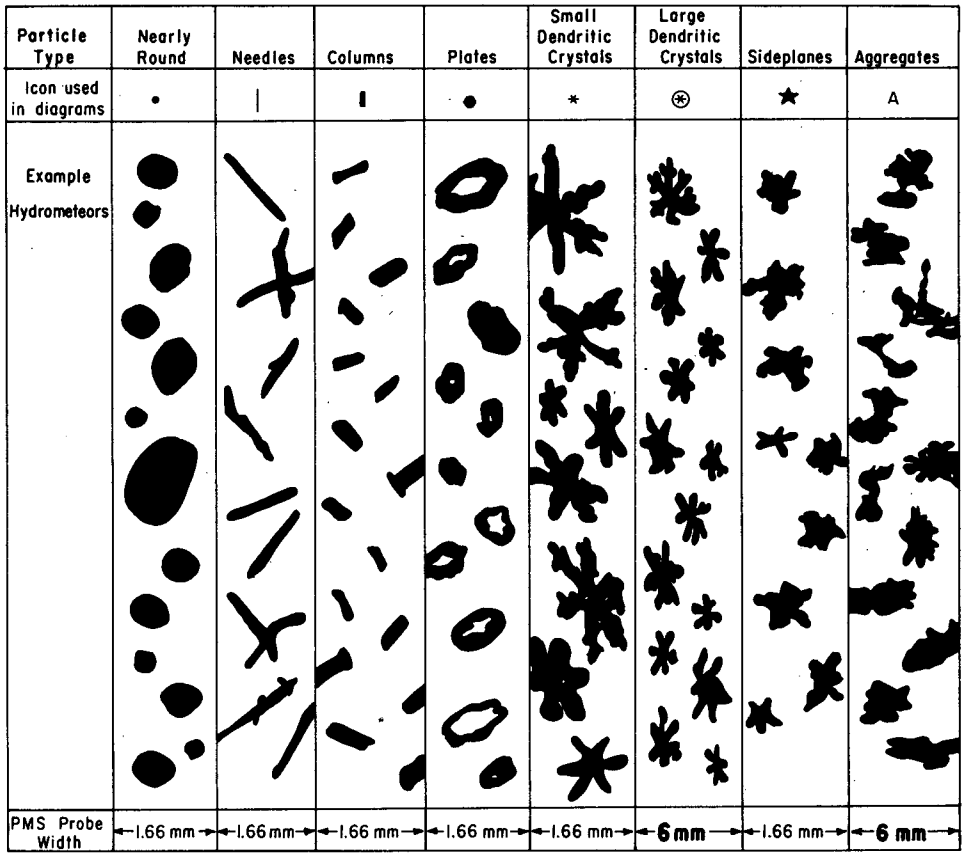

FIG. 1. Examples of ice particles observed during 3–8 July by PMS probes. Icons are used in the microphysical diagrams of this paper to depict various particle types. The icon for each type is shown.

the frequency of occurrence of particles of each of the identified types are illustrated by plotting icons at each 1 min segment of the flight track. The first such illustration is Fig. 2d. Since the typical ground speed of the P3 was 10 km min^{-1}, each 1 min sample of microphysical data represents a distance of about 10 km. A single icon is plotted if 10–29 particles of the specified types were observed in that increment of the flight track. If 30 to 49 particles were observed during 1 min, two icons are plotted. Three icons represent 50–69, and four indicate 70 or more identified particles. If 0 to 9 particles were observed, no icon was plotted. The exception to this rule is that one icon was plotted wherever at least 1 large dendritic crystal was observed in a 1 min period.

These frequencies can be converted approximately to concentrations by dividing by the flow rate through the PMS probes. The flow rate for the cloud probe was about 22 L min^{-1}, for the precipitation probe 283 L min^{-1}. *Caveat emptor,* since only the identifiable particles (which account for only some 1% of the total particles encountered) are included in these frequency counts, resulting particle concentrations will be two orders of magnitude smaller than total particle concentrations. Thus, it would be fruitless to compare concentrations of identifiable particles with total concentrations in other studies.

Despite careful analysis, some hydrometeors are bound to have been classified incorrectly owing to lack of resolution in the images. For example, a column viewed on end might appear to be nearly round, a plate viewed on edge might be judged a column, or a splinter from a branched crystal might be seen as a needle. Although errors introduced thereby into the statistics discussed in section 4 are difficult to quantify, it is our impression that they do not have a significant impact on the conclusions of our study.

c. *Satellite data*

Satellite imagery was obtained from polar orbiting meteorological satellites of the United States Air Force's (USAF) Defense Meteorological Satellite Program (DMSP) in the form of photographic mosaics on microfilm. The mosaic images at infrared and visible wavelengths had 5-km resolution and were obtained twice daily. Only visible images are used in this paper.

d. *Other data*

Dropwindsondes from both the P3 and the NCAR Electra aircraft provided vertical soundings over the Bay of Bengal. These soundings, as well as continuous flight-level data from the P3, such as temperature, humidity, cloud liquid water content, altitude and horizontal and vertical wind velocities, were obtained on microfilm. This information is available through the World Data Center A, National Climatic Center, Asheville, North Carolina, 28801.

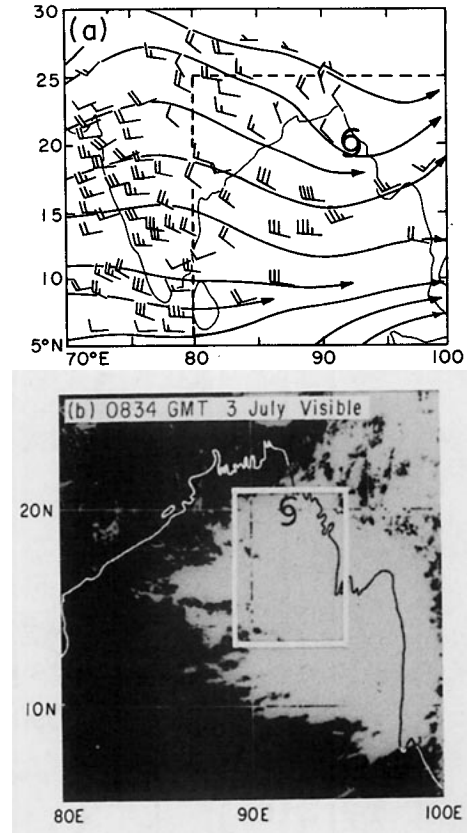

FIG. 2. Data for 3 July 1979. (a) 850 mb winds and streamlines at 1200 UTC based on surface and aircraft measurements (one full barb represents 5 m s^{-1}). Adapted from Krishnamurti et al. (1980). The approximate position of the surface low is indicated in each panel of this figure by the hurricane symbol. The dashed box identifies the area covered by the satellite picture shown in panel b. (b) Visible DMSP satellite mosaic image for 0834 UTC 3 July. The box delineates the area of radar observation shown in panel c and microphysical observations in panel d. (c) Radar composite. Shading thresholds are at 1, 20, 30 and 35 dBZ. Flight track of the P3 is indicated by the dashed and solid lines. The solid line indicates portions of the flight path where radar data were collected, and from which the composite was generated. Dashed line shows portions of the flight track where radar were not being collected. Numbers indicate times (UTC) every 15 min at the corresponding hash marks on the flight track. The heavy, bold curve outlines the area over which radar data were obtained. The scalloped line indicates approximate cloud boundaries, based on satellite imagery in panel b and microphysical observations of panel d. (d) Microphysical observations. Solid and dotted lines indicate flight track of the P3. Solid indicates regions where particles were detected by PMS probes and recorded on tape. Dotted indicates flight track where no particles were recorded. Times (UTC), flight level (km), and flight-level temperatures (°C), are indicated every 15 min at hash marks along the flight track. The icons along the flight track indicate the identifiable hydrometeor types, and, as explained in section 2, frequencies of observation for every 1 min period of flight are indicated by the number of icons presented side by side. See Fig. 1 for a legend of particle types. Scalloped lines repeat the approximate cloud boundaries shown in panel c.

3. Daily radar and cloud microphysical structure

In this section, we present day-by-day descriptions of the substorm-scale structure of the clouds and pre-

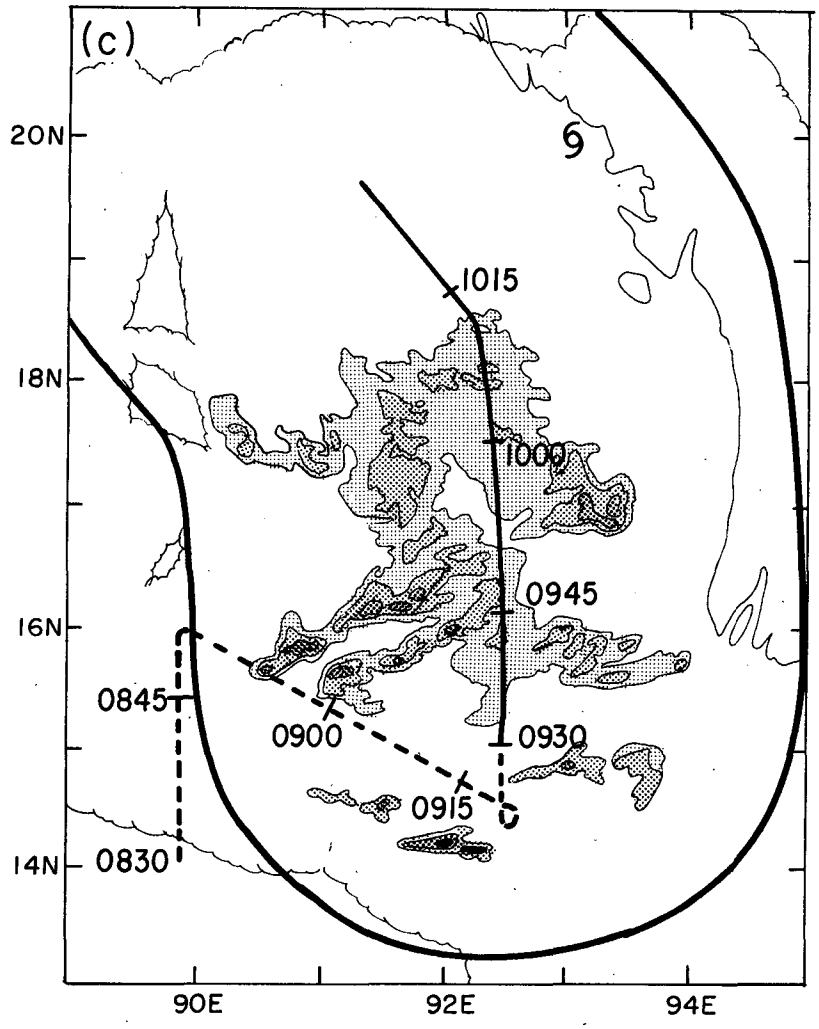

FIG. 2. (*Continued*)

cipitation in the monsoon depression as seen in satellite cloud images, radar depictions of the precipitation areas and cloud microphysical measurements taken along the flight tracks. The purpose of these descriptions is to demonstrate that

- Precipitation was concentrated in mesoscale precipitation features that were 100–500 km in horizontal dimension and tended to be elongated roughly in an east–west direction. No evidence is seen of precipitation on horizontal scales large enough to suggest that they were being produced directly, either wholly or in part by storm-scale ascent, nor was the pattern one of an ensemble of purely convective-scale elements.
- The time scale of the rain areas in the depression was also mesoscale. Although the large-scale wind structure of the depression vortex changed little in structure from day to day, the pattern of mesoscale precipitation features within the storm was highly transient. The rain areas on a given day bore little resemblance to those on previous or succeeding days. This observation suggests again that the storm-scale ascent was not directly producing the precipitation. Yet the pattern of rain areas during a given 5–10 h flight period changed only slightly. Thus, the time scale implied for the rain areas was commensurate with their horizontal spatial scale.
- The mesoscale precipitation features of the depression contained large stratiform regions manifested as areas of 10s to 100s of km in dimension, over which relatively uniform echo of weak to moderate intensity was observed and where rather similar ice particle types were observed continuously. These large stratiform regions were attached to groups or lines of convective cells. This structure, together with the temporal and horizontal spatial scales seen in the daily patterns, suggest that the precipitation pattern in the depression was a continually varying ensemble of mesoscale features similar to those of the cloud clusters seen in GATE and Winter MONEX.

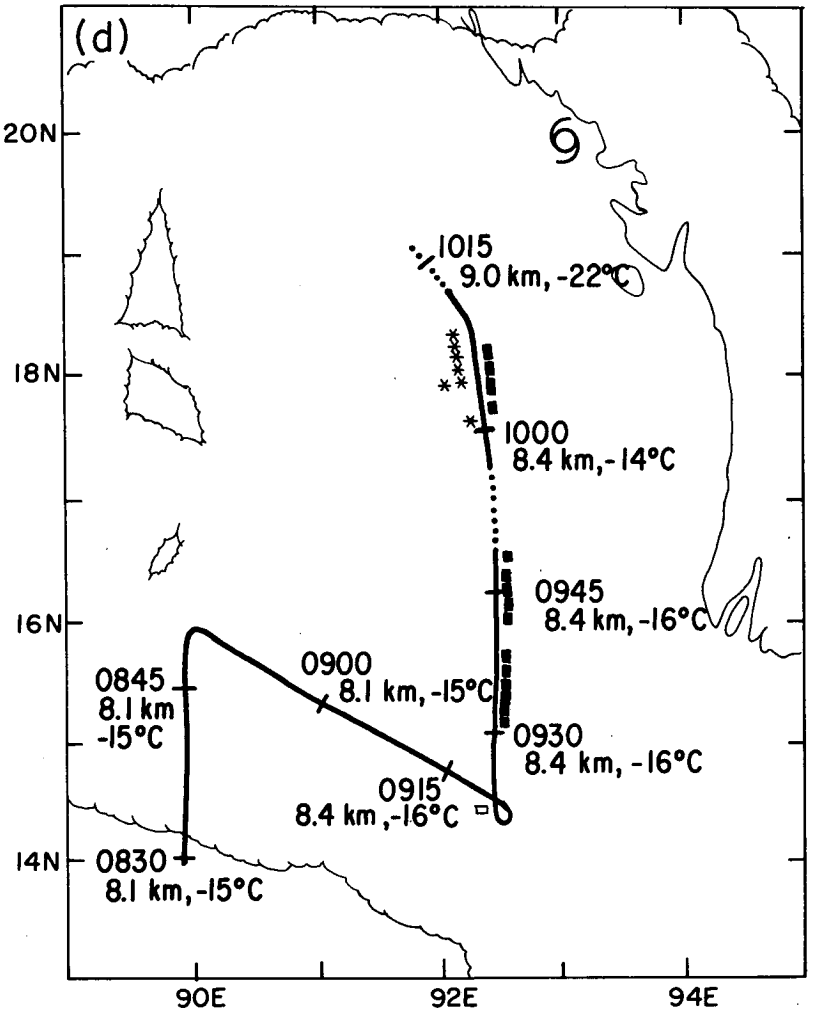

FIG. 2. (*Continued*)

• The larger of the mesoscale precipitation features tended to be elongated in the west–east to northwest–southeast direction.

a. 3 July

On 3 July (Fig. 2a) a trough extended from about 25°N, 95°E south and west into the Bay of Bengal, near 10°N, 90°E. Winds over the Bay at 850 mb, measured by dropwindsondes, were generally westerly at 15–20 m s^{-1}. They formed a trough on the east side of the Bay but did not yet indicate a closed circulation. The trough line coincided with a mesoscale cloud feature, centered near 15°N, 95°E, which dominated the cloudiness over the Bay (Fig. 2b). The P3 flew through this feature along the track shown in Figs. 2c and 2d. The cloud boundaries in panel b were used to sketch the nephanalysis (indicated by scalloped lines) in panels c and d. The cloud boundaries were slightly modified in places in order to be as consistent as possible with the microphysical observations of panel d and the radar echoes of panel c. Cloud boundaries in later figures were constructed in a similar manner.

Radar data were recorded beginning at 15°N, 92.5°E, while microphysical observations were obtained starting earlier at 14°N, 90°E. Since the radar observations were not recorded for the full duration of this penetration, the echo pattern shown in Fig. 2c does not quite fully represent the structure of the precipitation features penetrated. The radar nonetheless showed the following features: convective cells in the region 14°–15°N, 91°–94°E; two nearly parallel lines of convection oriented northeast to southwest near 16°N, 91°–92°E; and a region of stratiform precipitation extending northward to 19°N, and eastward to 94°E. The region of stratiform precipitation is much larger than the areas of convective cells. The stratiform region consisted of two northwest–southeast-oriented bands. As will be seen in the radar data for subsequent days, this elongation and orientation was rather typical of the larger mesoscale precipitation features in the

depression. The mesoscale precipitation area was located beneath the dense high-level overcast seen in the satellite picture. This large cloud shield was probably the merged canopies of several mesoscale features.

The radar data in Fig. 2c indicate that the primary rain area seen from the aircraft was 100–400 km in horizontal scale. The convective lines extending from the larger area were 50 km in the cross-line dimension, and the isolated convective groups outside the main rain area were also about 50 km across. These scales are similar to the scales of the rain areas seen in cloud clusters (Houze and Betts, 1981; Houze et al., 1981b; Churchill and Houze, 1984a). The tendency for most of the rain area to be composed of less intense and less variable stratiform precipitation is also similar to cloud clusters.

Microphysical observations are indicated in Fig. 2d. Solid lines in this and subsequent microphysical panels indicate flight through regions where the PMS probes detected hydrometeors. Dotted lines indicate regions where the PMS probes detected no particles. Particle concentrations along the solid lines ranged from 0.9 L^{-1} at cloud edge to 740 L^{-1} at 1000 UTC. Almost the entire in-cloud flight track, except for a brief period between 1000 and 1005 UTC, was in stratiform cloud.

Although the aircraft was close to several intense radar-echo cells at the ends of the two lines extending southwest from the main rain area (between 0845 and 0930 UTC), none was penetrated (Fig. 2c). All of the PMS data was taken within the large, apparently stratiform region of the main rain area. From about 0832 to 0855 UTC, columns, small dendritic crystals and nearly round particles were observed in this region, but too infrequently to be indicated on the diagram. Columns were frequent from 0931 to 0947 UTC. From 1001 to 1009 UTC small dendritic crystals were abundant, and columns were again present. These branched crystals were evident over a distance of 50 km, while the columns were continuously observed over distances of 50–100 km. These horizontal scales over which rather uniform microphysical characteristics were observed are consistent with the interpretation, based on radar-echo structure, that this portion of the precipitation area was stratiform rather than convective in character. Rather homogeneous microphysical structure was also seen in the stratiform-appearing echoes of Winter monsoon cloud clusters (Houze and Churchill, 1984).

In the convection encountered between 1000 and 1005 UTC, vertical air motions averaged over 1 s intervals frequently exceeded 5 m s^{-1}. A peak 1-s value of 18 m s^{-1} was observed. The altitude of the aircraft was about 8.5 km, and the temperature was −15°C. Liquid water contents were very small ($\leq$0.1 g m^{-3}). Low liquid water contents at similar altitudes were found in the convective updrafts of cloud clusters observed during Winter MONEX (Churchill and Houze, 1984a,b; Houze and Churchill, 1984).

b. 4 July

On 4 July, no aircraft missions were flown, so radar and cloud microphysical data were not collected. The low-level wind field (not shown) indicated a circulation center, marking the birth of the depression, at the head of the Bay near 20°N, 92°E.

c. 5 July

On this day, the low-level circulation center was near 20°N, 91°E (Fig. 3a). The precipitation detected by radar (Fig. 3c) was located generally west and south of the surface depression center. This location was characteristic of the precipitation in this storm on each of the days we have examined. Godbole's (1977) composite analysis of monsoon depressions over land found

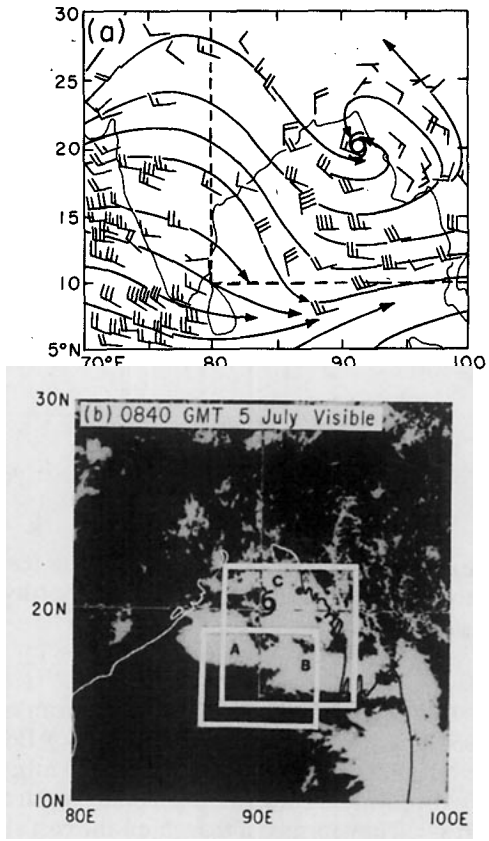

FIG. 3. Data for 5 July 1979. (a) Same as Fig. 2a, but for 5 July. (b) Visible DMSP satellite image for 0840 UTC 5 July. Large box denotes area covered by the radar composite of panel c. Small box denotes area covered by the radar composite of panel e. Capital letters help identify the same features in different panels. (c) Southbound radar composite. Same format as Fig. 2c. (d) Southbound microphysical observations. Same format as Fig. 2d. (e) Northbound radar composite. Same format as Fig. 2c. Microphysical observations are also included. Graupel was observed shortly after 1000 UTC, and a shower of sideplanes just before 1030 UTC. Ice particles were observed continuously along the flight track from southern edge of the cloud boundary to the northern edge.

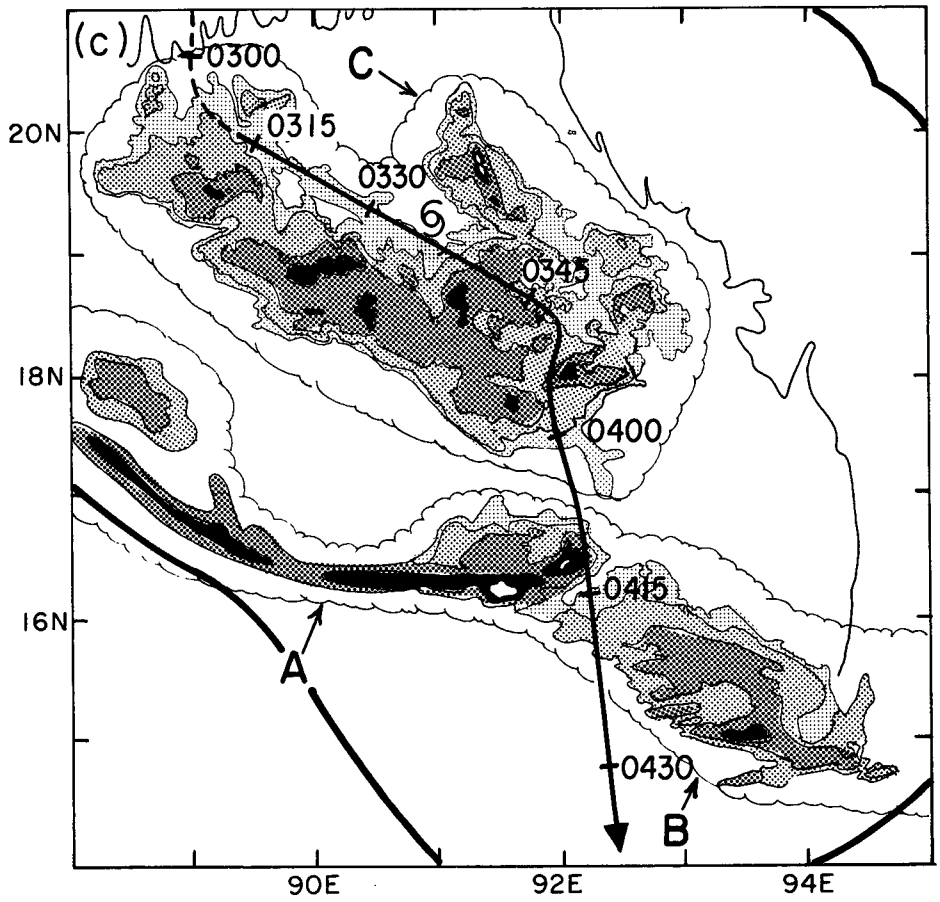

FIG. 3. (*Continued*)

that precipitation was located preferentially west and south of the surface low. It thus appears that the location of precipitation relative to the storm center over the Bay was the same as it typically is over land.

Within the larger-scale pattern of clouds and rain, three distinct mesoscale features (labeled A, B and C) were evident. All were oriented northwest–southeast. In the satellite image (Fig. 3b), feature A extended south and east from 20°N, 87°E to 18°N, 90°E, where it was connected to feature B, which extended east to 17°N, 96°E. Feature C was centered near 20°N, 92°E.

In the radar echo pattern (Fig. 3c), feature A appeared as a narrow line of intense, apparently convective precipitation about 500 km long and 20–50 km wide, arcing east to northwest, with maximum reflectivities exceeding 40 dBZ. Feature A was encountered again on the northbound leg of the flight between 0945 and 1115 UTC (Fig. 3e). It had moved to the south-southeast about 190 km during the 5.5 h between penetrations. As pointed out by Warner (1984b), the mean speed of this feature (9–10 m s^{-1}) was similar to the speeds of the convective lines of squall-type cloud clusters that occur in lower latitudes (e.g., Zipser, 1969, 1977; Houze, 1977; Gamache and Houze, 1982). The occurrence of stratiform cloud and precipitation to the rear of these lines is typical. On the earlier, southbound flight leg (Fig. 3c), patches of lighter, apparently stratiform precipitation, 50–100 km in dimension, were located to the north (i.e. rear) of this line on both its eastern and western ends. When the aircraft entered the convective line at its new southward location at about 1000 UTC (Fig. 3e), the line was trailed by a 200-km wide stratiform cloud deck (note from the solid portion of flight track that ice particles were being detected continuously from 0957–1030 UTC).

To the southeast of feature A, feature B seen in Fig. 3c appeared to consist primarily of a stratiform precipitation area 200–400 km in horizontal dimension. Feature C, located to the north of A and B, consisted of a mesoscale area of rain 500 km long and 100–200 km wide. Within C, convective cells were embedded in a large region of stratiform precipitation.

A 300 km segment of a stratiform portion of feature C was traversed by the P3 from about 0300 to 0345 UTC (Fig. 3d). The flight level was just above the 0°C level, and the stratiform character of the precipitation region was underscored by the section of the flight between 0330 and 0345 UTC, where rather similar par-

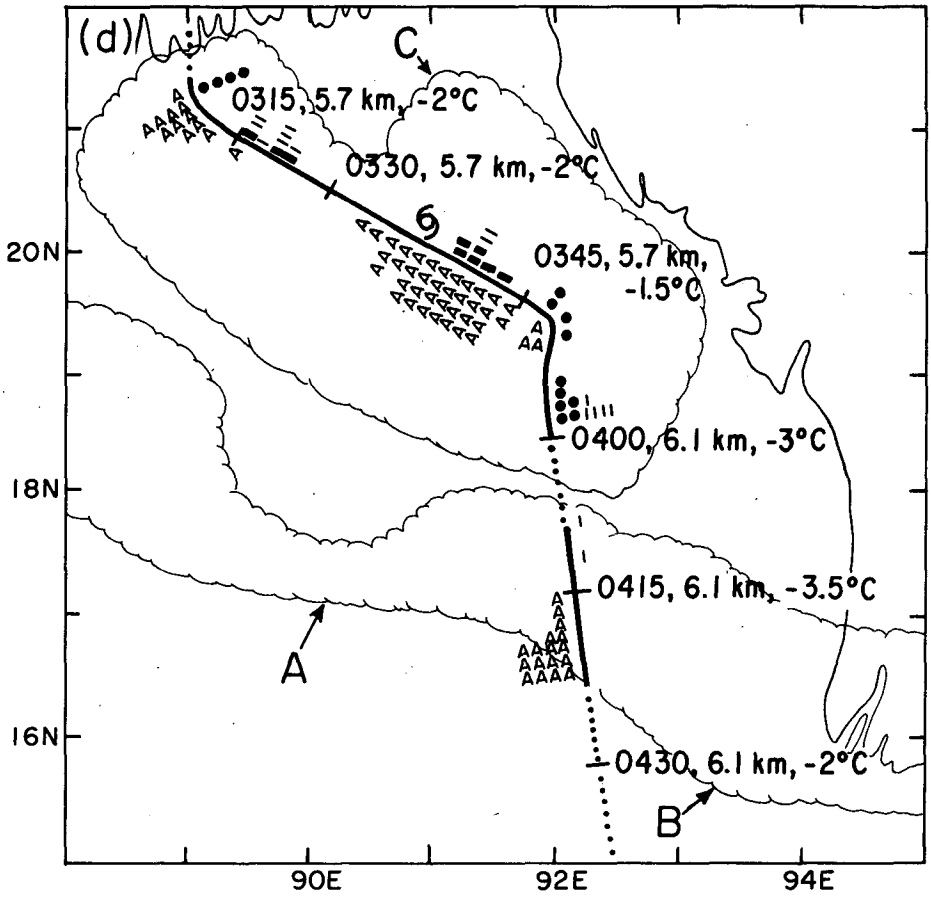

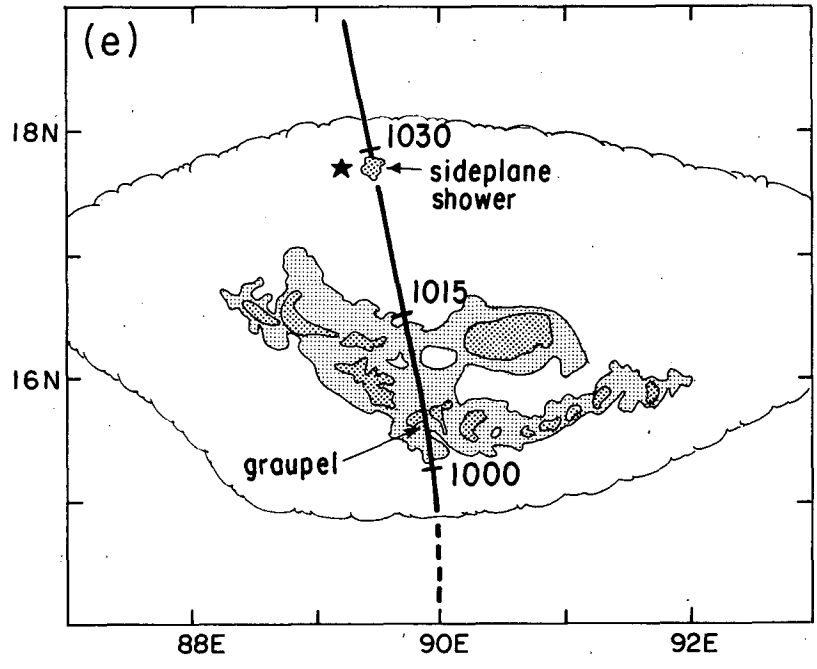

FIG. 3. (*Continued*)

ticle characteristics, highlighted by the occurrence of numerous large aggregates, were observed continuously for some 150 km. Needles and columns were also seen in this region. Large dendritic crystals were also prevalent throughout this region.

From about 0350 to 0358 UTC, the P3 passed through a convective portion of feature C. Several cells appeared to be embedded in the surrounding stratiform precipitation, and peak updrafts ≥ 5 m s^{-1} were noted as the aircraft passed around the edge of a convective core near 19°N, 92°E. Warner (1984b) presents additional statistics on convective updraft speeds and durations in this region. The convective cells encountered were characterized by both needles and nearly round particles. Many of the nearly round particles seen along this segment of flight track appeared to be liquid-water drops, characterized by a smooth, nearly circular appearance in the two-dimensional particle images. Flight-level temperatures were averaging −2°C, but there were periods when the flight level temperatures rose to within 0.5 deg of 0°C. We suspect that the temperature sensors on the P3 were accurate to within no more than a degree, so the P3 may have been flying through warm cloud when drops were observed. Some of the nearly round particles exhibited a lumpy character suggesting that they were either ice particles in the process of melting or graupel particles from the convective cells.

Feature B appeared on radar to be mostly stratiform (Fig. 3c). Its overall dimensions were about 100 km × 250 km, and the identifiable ice particle images seen between 0414 and 0424 UTC, as in the stratiform region of feature C (0300–0345 UTC), were predominately aggregates, with some large dendritic crystals. Very large concentrations of aggregates were seen continuously over a distance of about 80 km just after 0415 UTC. The east end of B was apparently more convective, as Warner (1984b) reported new cumulus towers building above flight level at that location.

When feature A was penetrated on the northbound leg of the flight (0945–1115 UTC), the P3 was at 9 km altitude, where the temperature was −20° to −23°C. For the most part, the particles encountered had no identifiable traits, although for a brief period in the convective line some small (diameter < 0.3 mm) nearly round particles were seen (1003 UTC in Fig. 3e). These particles were apparently small graupel lifted to flight level by the strong convective updrafts in the vicinity. At one location in the trailing stratiform cloud, just before 1030 UTC, branched crystals of the sideplane type (Fig. 1) were observed.

d. 6 July

On 6 July, the low-level circulation center was near 20°N, 90°E (Fig. 4a). Satellite data (Fig. 4b) show that four distinct mesoscale cloud masses (features D–G) were located southeast, southwest and northwest of the surface low.

The radar-observed precipitation areas associated with the large cloud masses D, E and G (Fig. 4c) were not as large as those seen on 3 and 5 July; those areas were 400–500 km in horizontal dimension (cf. Figs. 2c and 3c). The echo areas associated with D, E and G were nonetheless mesoscale in dimension, typically 100–200 km across, and again consisted of a mixture of convective and stratiform structure. Farther south, the precipitation area of feature F contained a 500 km long convective line, which resembled feature A on 5 July with its arc-shape and west-northwest–east-southeast orientation (cf. Fig. 3c).

All of the cloud traversed on the south-southwestward track through features D, E and F (from 0515 to 0630 UTC) appeared from the radar echo to be stratiform, and no convective vertical motions were encountered by the P3 during that time. On the zig-zag northbound flight track (0810–1015 UTC in Fig. 6d), the P3 penetrated the eastern edge of feature F and subsequently portions of features G and E. Again, all of the cloud penetrated was stratiform, and, as on the southbound track, the PMS probes detected hydro-

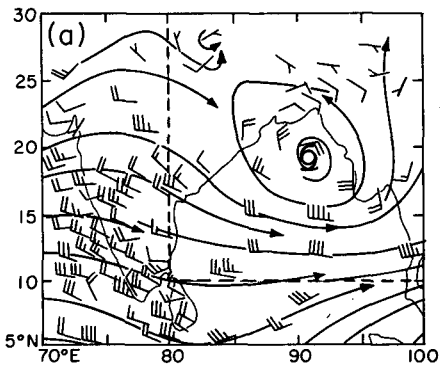

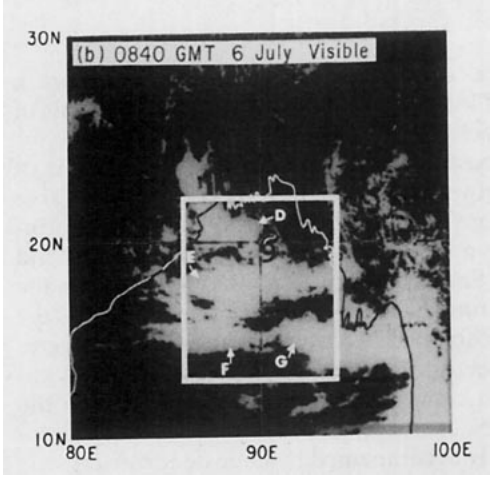

FIG. 4. Data for 6 July 1979. Same format as Fig. 2. Capital letters help identify the same features in different panels.

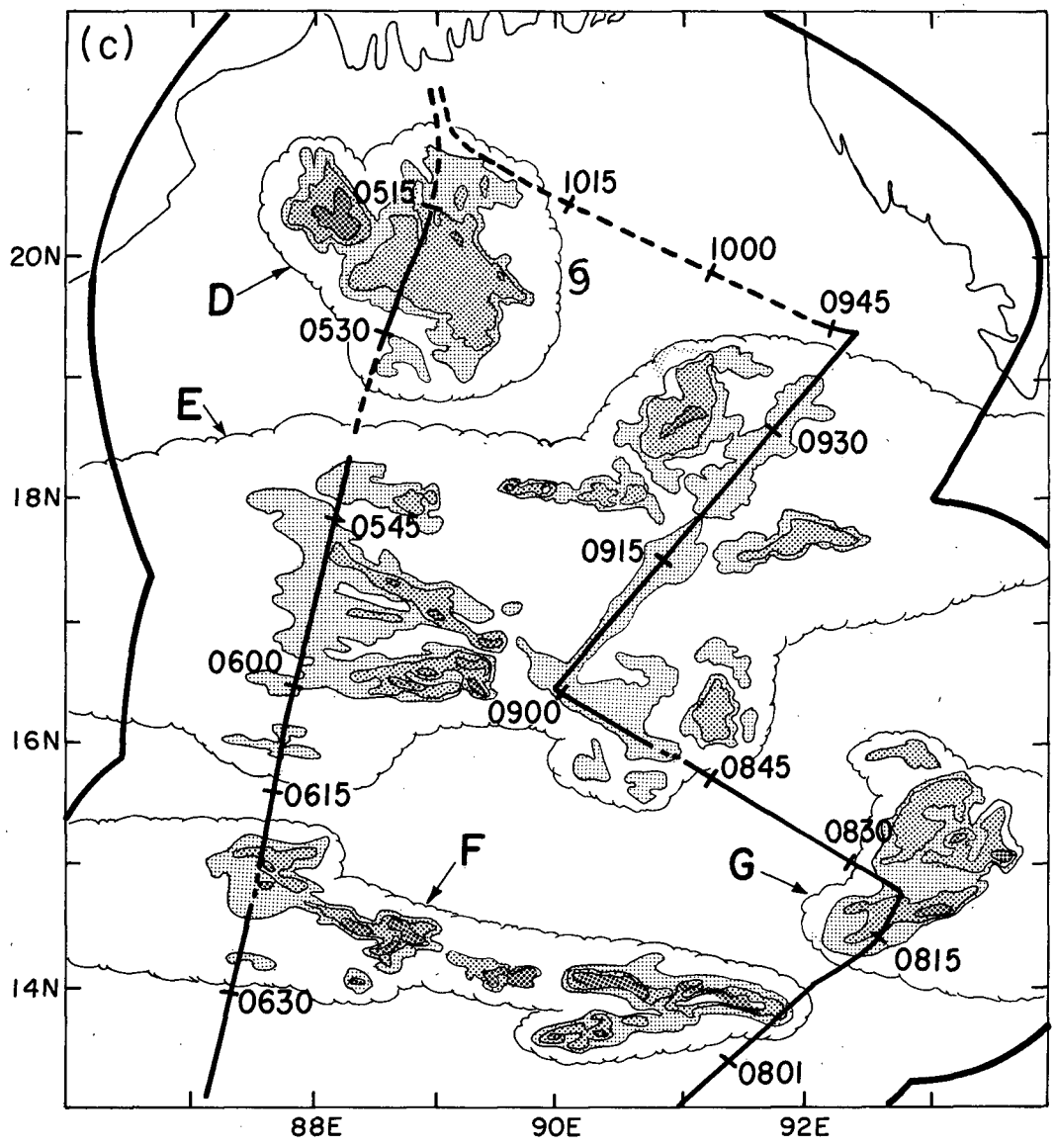

FIG. 4. (*Continued*)

meteors for continuous stretches of flight track hundreds of kilometers in length (the solid portions of the flight track).

The P3 passed through the stratiform segment of feature D between 0515 and 0530 UTC (Fig. 4d). Large concentrations of aggregates were encountered continuously over a distance of 50 km between 0520 and 0525 UTC. Similar observations were obtained as the aircraft continued south-southwestward through the stratiform echo areas of features E and F. Large aggregates were seen nearly continuously for over 400 km of flight path between 0535 and 0623 UTC. As in the stratiform regions observed on 5 July, the aggregates were regularly accompanied by large dendritic crystals (especially between 0600 and 0615 UTC). As will be discussed in section 4, these observations suggest that the aggregates were formed by the entanglement of large dendritic crystals.

Feature F was traversed by the P3 aircraft at both its ends. However, the aircraft detoured around intense convective cores, flying instead through mostly stratiform precipitation (Fig. 4c). Near the west end of the convective line, however, a few nearly round particles were seen (0627 UTC in Fig. 4d). These particles were probably graupel detrained from convective cells and subsequently mixed into the surrounding stratiform cloud.

In the stratiform regions of features F, E and G seen on the northbound flight track (0800–1015 UTC in Fig. 4d), aggregates and large dendritic crystals were

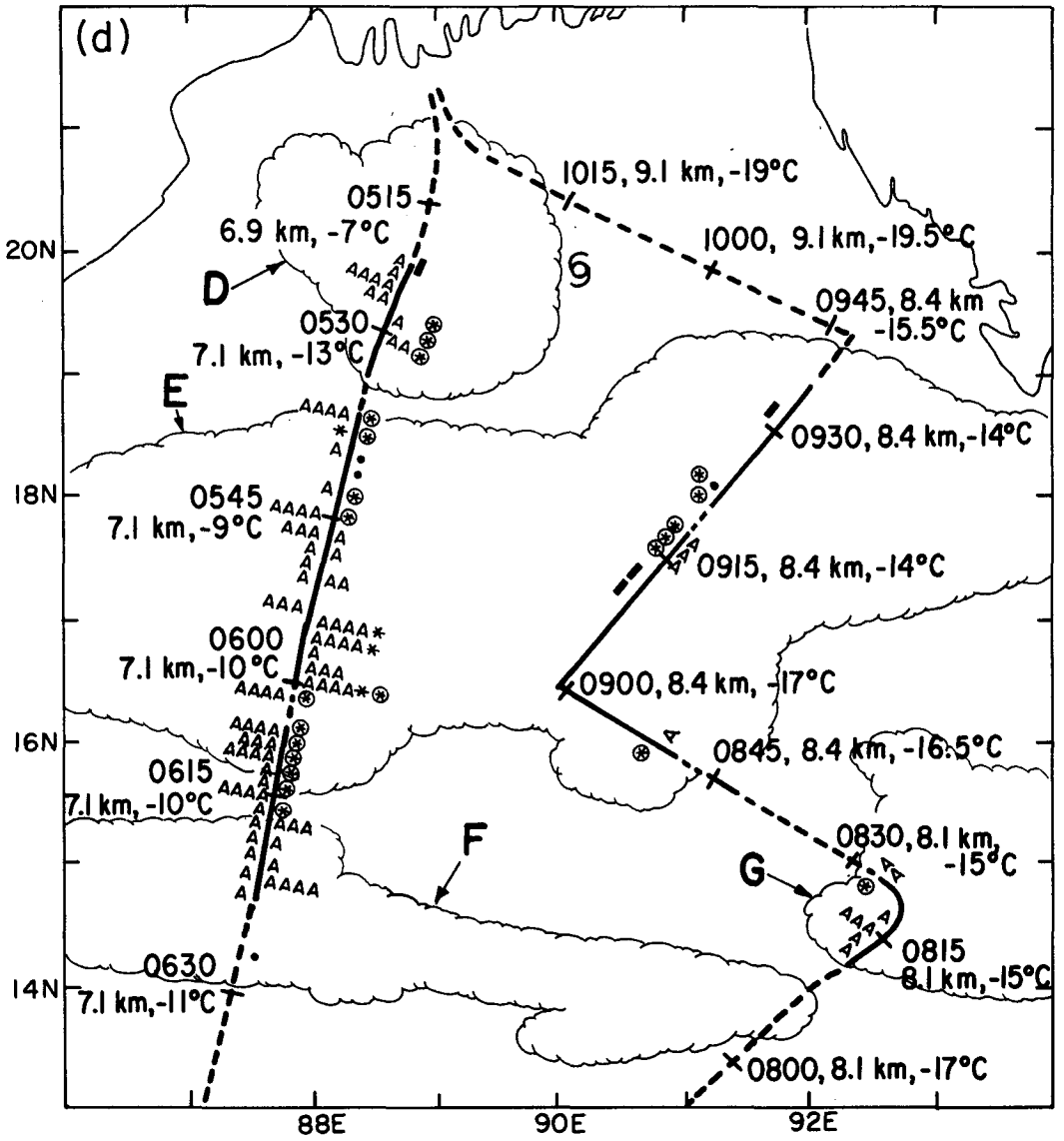

FIG. 4. (*Continued*)

again seen, although not in as great profusion as on the earlier southbound track. In feature E (0910–0931 UTC), columns and nearly round particles occurred sporadically among the aggregates and large dendritic crystals.

e. 7 July

On 7 July, the P3 operated in the vicinity of the depression center, which was located near 20°N, 89°E (Fig. 5a). Extensive areas of high cloud again were located southeast through southwest to northwest of the storm center (Fig. 5b).[3]

By locating overshooting cloud tops evident at low sun angles in visible satellite imagery, Johnson and Houze (1987) identified regions of deep convection between 85° and 90°E at 0526 UTC (features I, K and L in Fig. 5b). The pattern of high cloud towers defining features K and L again exemplifies the tendency for intense convective lines in the southern part of the depression to be oriented east–west and bow southward (cf. features K and L in Fig. 5b, A in Fig. 3c and F in Fig. 4c). Except for the overshooting towers, the cloud-top pattern in the depression, as on the other days, was dominated by huge stratiform (or "anvil") cloud structures corresponding to the major mesoscale features (e.g., see Fig. 5e). These widespread cloud shields apparently had midlevel bases. From photogrammetry of the clouds viewed from aboard the P3 aircraft, War-

[3] Note that panels b–g of Fig. 5 are arranged in chronological order.

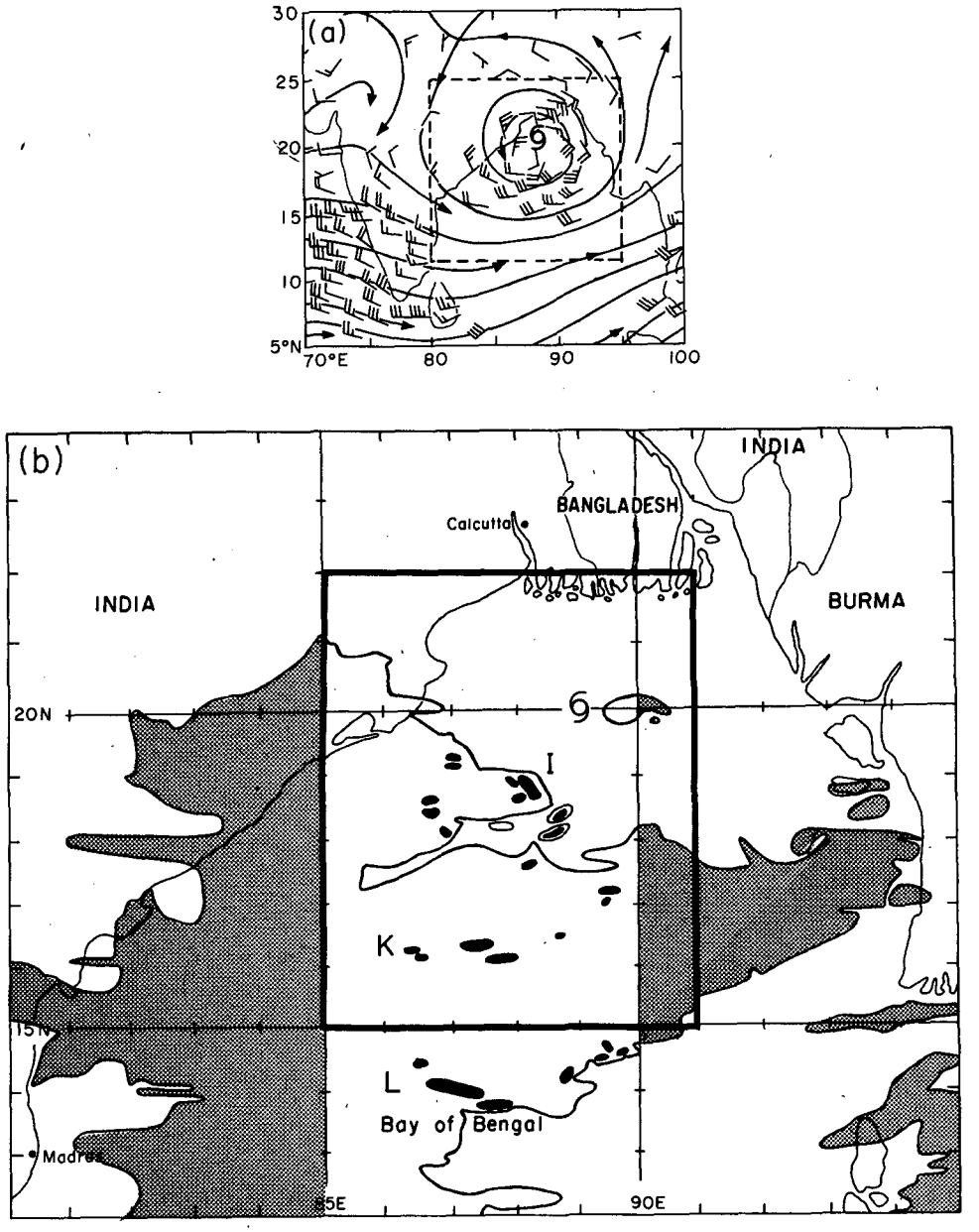

FIG. 5. Data for 7 July 1979. (a) Same as Fig. 2a, but for 7 July. (b) Nephanalysis based on DMSP satellite image for 0344 UTC. Adapted from Fig. 39 of Johnson and Houze (1987). Capital letters help identify the same features in different panels. The box shows area of radar composite in panels c and d. Shaded areas outline the infrared satellite cloud pattern at 0344 UTC, while in the unshaded region between 85° and 90°E, dark spots locate high convective cell tops, which were illuminated in the visible photograph on which panel b was based as a result of low sun angle. (c) Radar composite for low-level flight. Cloud boundaries based on 0344 UTC DMSP image. Same format as Fig. 2c. (d) Radar composite for midlevel flight. Cloud boundaries based on 0344 UTC DMSP image. Same format as Fig. 2c. (e) 0840 UTC DMSP visible image. Box denotes area of upper-level composite shown in panel f. (f) Radar composite for upper-level flight. Same format as Fig. 2c. (g) Upper-level microphysical observations. Same format as Fig. 2d.

ner and Grumm (1984) derived maps showing "extensive anvil cloud based at 400 mb, apparently arising from cumulus."

Warner and Grumm (1984) examined the satellite-observed cloud mass containing feature K in some detail and found that this northeast–southwest oriented feature consisted of a cloud band tracking east-northeastward with a highly convective leading edge that moved by discrete propagation, somewhat like a squall line.

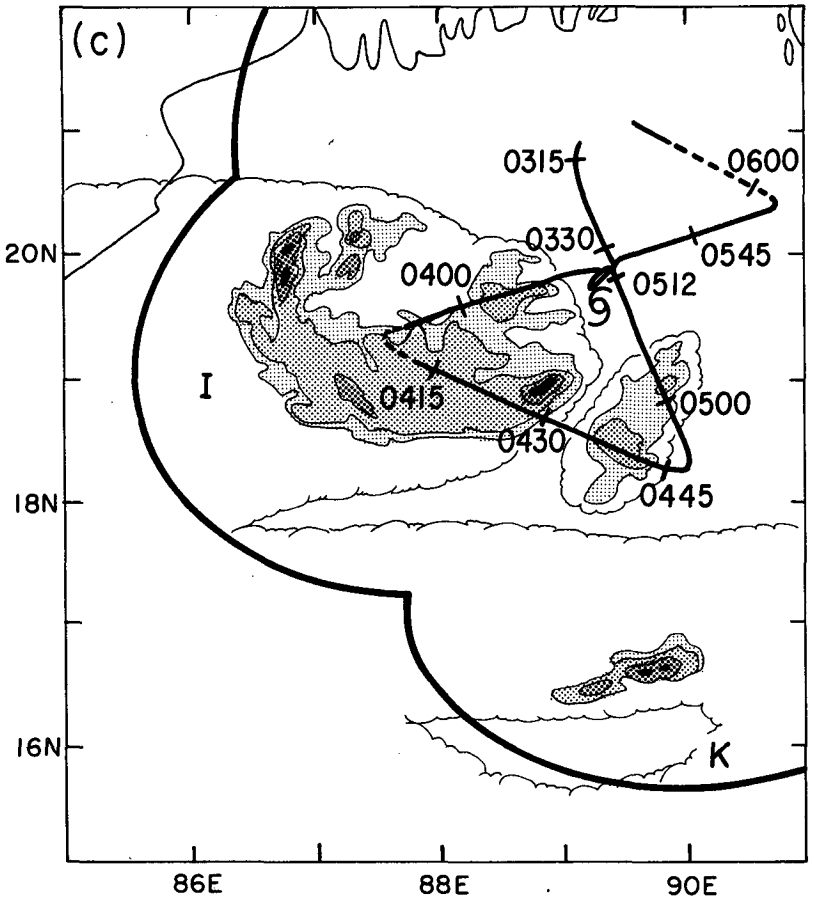

FIG. 5. (*Continued*)

The P3 executed low- and midlevel butterfly tracks near the center of the depression at approximately the times of the satellite pictures represented in Figs. 5b and e, respectively. The low-level track was at an altitude of 0.5 km, while the midlevel track was at 3 km. Composites of the radar echo patterns observed on these flights show in detail the mesoscale rain area associated with feature I (Figs. 5c and d). Feature I was a large area of moderate stratiform rain, 100 km × 300 km in dimension, with a roughly west-northwest–east-southeast orientation and embedded intense convective cells. The strongest cells tended to be on the east end of this feature.

An upper-level flight leg was flown at an altitude of 7.8 km in stratiform regions of features I and J (Fig. 5f). Because of the altitude, the radar was detecting the upper portions of precipitation-filled volumes, and echoes were therefore not as widespread or as intense as those seen on the lower-level flight legs. The PMS probes detected ice particles continuously for distances of over 100 km between 0924 and 0928 UTC and 300 km between 1020 and 1048 UTC (Fig. 5g). These distances again indicate the mesoscale dimensions of the primary precipitation features in the depression. As in other mesoscale stratiform regions of the depression, aggregates and large dendritic crystals were frequently observed. At around 1030 UTC, sideplanes were seen. Sideplanes were noted frequently at similar altitudes in the stratiform regions of Winter MONEX cloud clusters (Houze and Churchill, 1984).

f. 8 July

By 8 July, the depression center had moved inland over India (Figs. 6a and b). Although the primary area of cloud cover remained south and west of the storm center, two lines of west–east-oriented cloud and precipitation southeast of the center (features M and N in Fig. 6c) were over the Bay, and both of these were penetrated by the P3. As on previous days, the lines were oriented generally east to west and were 100–300 km in horizontal dimension.

On its passage through feature M (0344–0416 UTC), the P3 encountered mostly stratiform precipitation. The temperature range was 0° to −1°C, and needles, nearly round particles and columns were dominant identifiable particle types. The nearly round particles had some straight edges and sharp corners, which sug-

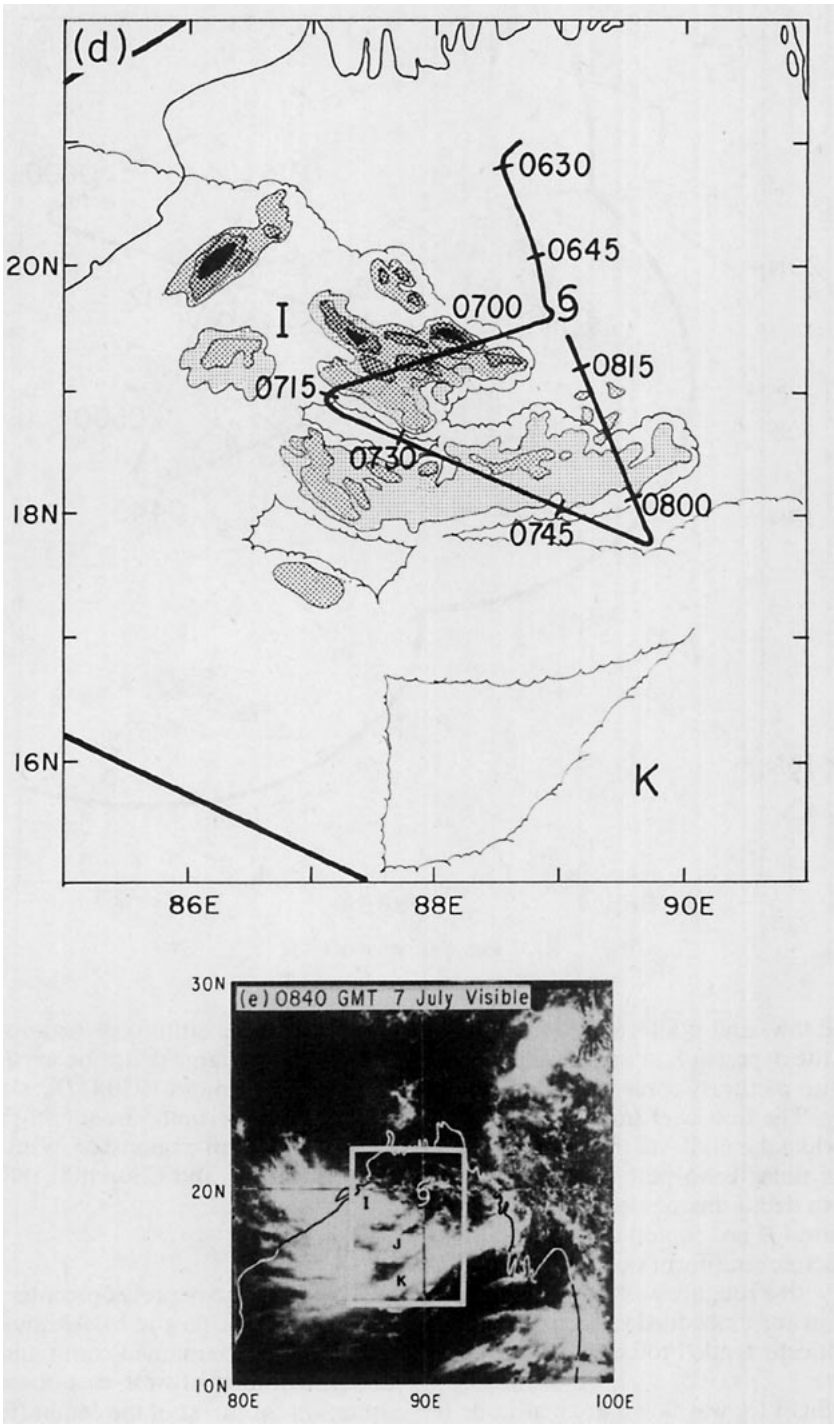

FIG. 5. (*Continued*)

gested they were rimed ice particles. At 0415 UTC, however, the nearly round particles increased in number and became very smooth in appearance, indicating they were raindrops.

The P3 climbed to 6.4 km before entering feature N at about 0425 UTC. Once again, the aircraft flew through a stratiform region of the precipitation, and aggregates and large dendritic crystals were observed. A few plates were seen. Some of the large dendritic crystals were over 5 mm in diameter.

On the return leg (after 0500 UTC), the P3 descended to about 4.8 km, where the temperature was about

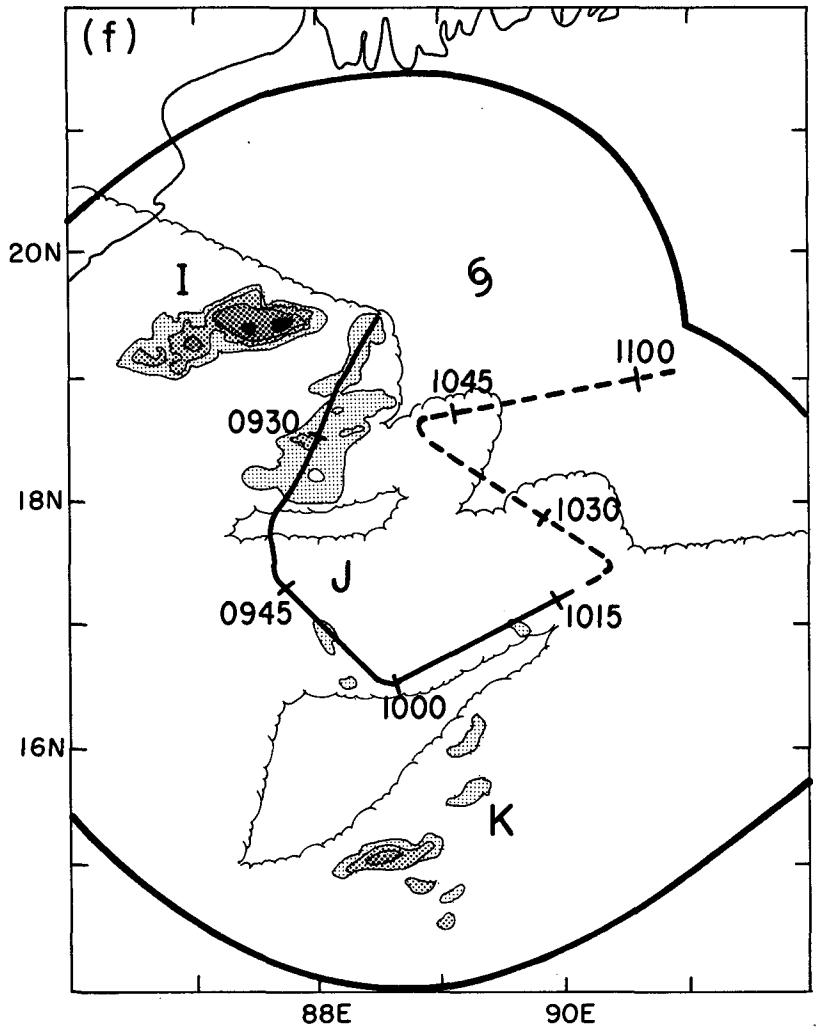

FIG. 5. (*Continued*)

+4°C. Both features were again penetrated, and the hydrometeors all appeared to be rain.

4. Vertical distribution of ice particles

In the analyses for individual days (sections 3a–f), we have seen that the rainfall from the Bay of Bengal depression was concentrated in mesoscale precipitation features 100–500 km in dimension containing both convective cells and regions of apparently stratiform rain, and that most of the flight tracks through precipitation areas were in these stratiform regions. Because of the large sizes of the stratiform areas, the flights were frequently within cloud continuously over distances exceeding 100 km, and they were conducted at altitudes with flight-level temperatures ranging between +5° and −25°C. Because of this extensive sampling over a wide range of flight altitudes, the PMS data obtained aboard the P3 provide a unique opportunity to examine the vertical distribution of ice particle types in the stratiform regions of the mesoscale precipitation features of the depression and thereby to infer the types of precipitation growth mechanisms that were operative in those regions. This analysis of the vertical distribution of microphysical processes deduced from direct measurement of the particles confirms that the dominant precipitation growth mode in the regions that appeared stratiform, in the horizontal maps of reflectivity and microphysical data examined in the previous section, was indeed stratiform and not convective in character.

An analyst was trained and employed to identify and count the particle images seen in the PMS data and to tabulate the results. By intention, however, this analyst was not cognizant of known relationships between ice particle growth temperature and particle habits. Hence, we believe the analyst was unbiased in

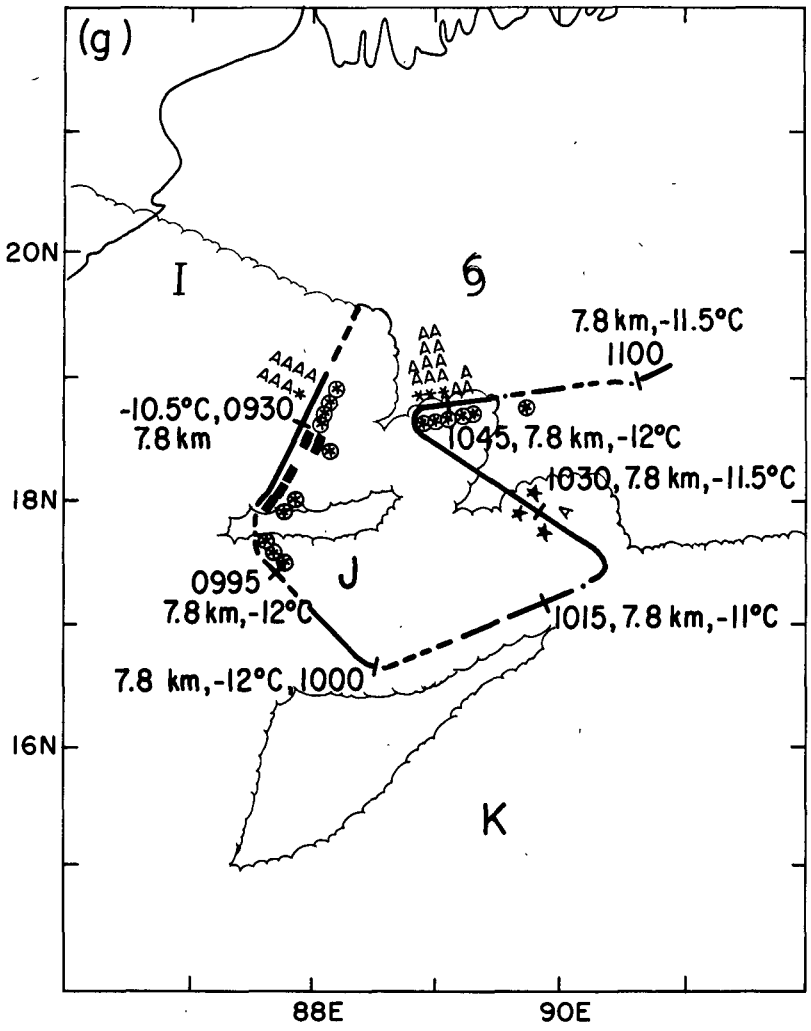

FIG. 5. (*Continued*)

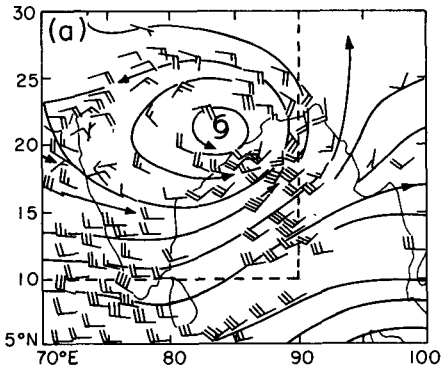

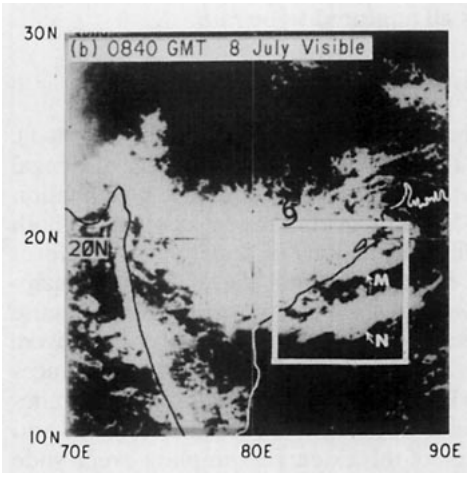

FIG. 6. Data for 8 July 1979. Same format as Fig. 2. Capital letters help identify the same features in different panels.

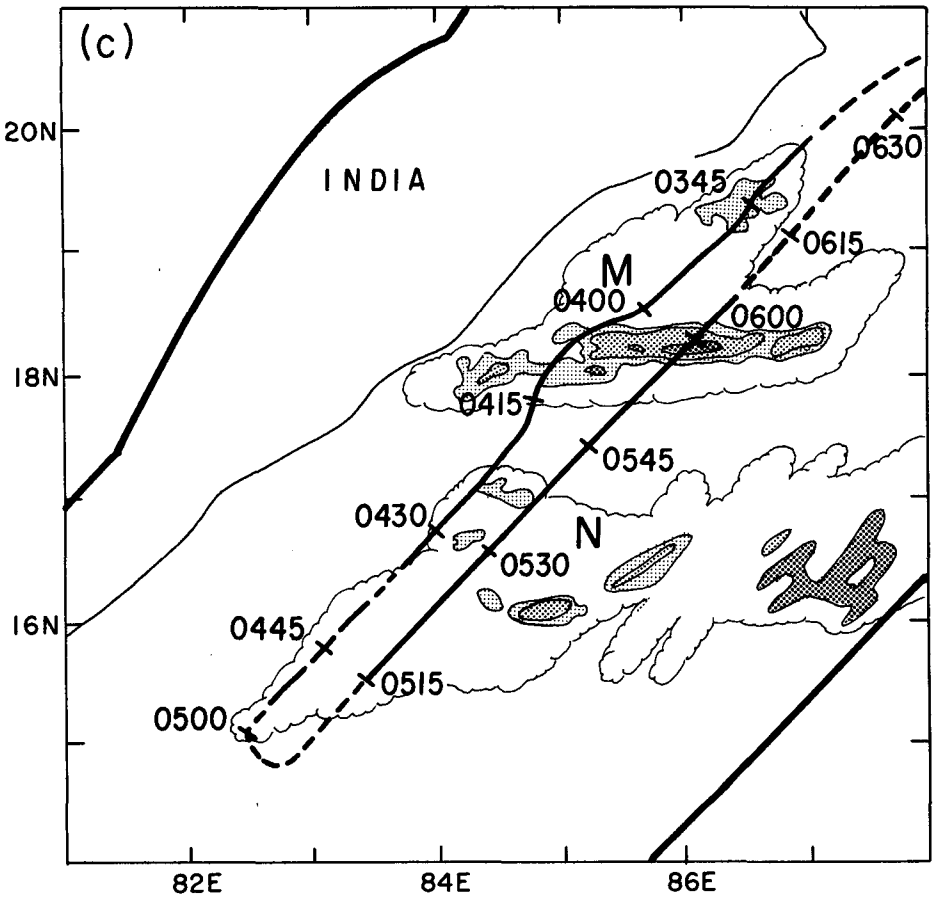

FIG. 6. (*Continued*)

identifying particle types, and this lack of bias has led to a fair, "blind" statistical study of the observed particle types in relation to flight-level temperature.

Data from all of the flights discussed in sections 3a–f are combined in Table 1, where they are grouped according to flight-level temperature and observed particle type. The data from flight tracks through regions of convective cells (0959–1001 UTC 3 July, 0353–0354 UTC 5 July and 1005–1007 UTC 5 July) have been omitted. For a given temperature range and particle category, we divided the total number of observed particles by the number of minutes that the aircraft was in cloud. The resulting mean concentration, in units of number per minute is indicated in Table 1 for each particle type and temperature range.

The data in Table 1 are presented graphically in Fig. 7. The vertical distributions shown are highly consistent both with each other and with the expected structure of precipitating stratiform clouds. The particle types in Figs. 7a and b have identifiable crystal habits, which are known to grow at certain ambient temperatures. If the particles fell about 1 km from their altitude of growth before being encountered by the aircraft,[4] then their growth temperature would be expected to be about 6°C lower than the flight-level temperatures indicated in Fig. 7 and Table 1. For example, a flight-level temperature of −5°C would correspond to an ice particle growth temperature (T_G) of about −11°C. The following discussion will demonstrate that the maxima and minima of the curves in Figs. 7a and b occur at temperatures that are consistent with about this amount of downward displacement of the ice particles from their level of origin.

The concentration of needles (Fig. 7a) was maximum at a flight-level temperature of −2°C. For one kilometer of sedimentation, the particles would have formed at a T_G of about −8°C, which is within the temperature regime in which needles are formed.[5] The vertical dis-

[4] This amount of downward particle displacement would require about 15 min at a fallspeed of 1 m s^{-1}.

[5] The temperature and humidity conditions for the growth of natural snow crystals are well known. The nucleation temperatures we refer to in this discussion were obtained from Fig. 10.11 of Hobbs (1974).

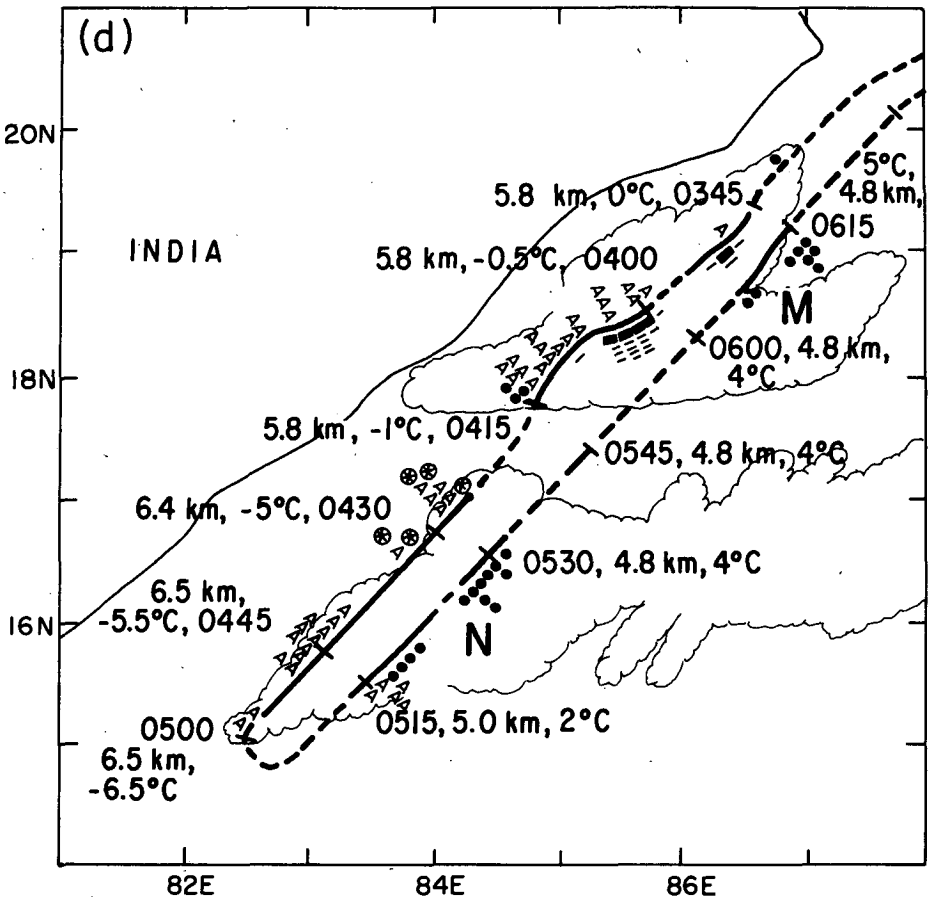

FIG. 6. (*Continued*)

tribution of columns is characterized by maxima at −2° and −18°C (or T_G = −8° and −24°C). These temperatures correspond to the two favored temperature regimes of columnar crystal growth in the atmosphere. These occur at T_G = −8° to −10°C and T_G = −20° to −28°C.

Figure 7b displays the vertical distributions of plates, small dendritic crystals and large dendritic crystals. The distributions of plates and small dendritic crystals closely parallel each other. This similarity is reasonable since branched crystals, especially dendrites, stellars, sector plates and the like, are actually modified plates. The plates, small dendritic crystals and large dendritic crystals share the same flight-level temperature of maximum concentration (−7°C). The peak is particularly well-marked for the large dendritic crystals. The corresponding growth temperature, for 1 km of sedimentation, is T_G = −13°C, which falls within the primary regime of natural branched crystal growth (T_G = −12° to −17°C). The maximum of large branched crystal concentration is rather broad, extending over flight-level temperatures of about −7° to −12°C, corresponding to growth temperatures T_G = −13° to −18°C, which agrees very well with the natural growth regime.

The two maxima for columnar crystals seen in Fig. 7a straddle the level of maximum concentration of plates, small dendritic crystals and large dendritic crystals seen in Fig. 7b. This comparison is consistent with the known tendency for the production of crystals to vary from prismlike at T_G = −4° to −10°C to platelike at T_G = −10° to −22°C back to prismlike at T_G < −22°C (see Table 4.2 of Wallace and Hobbs, 1977).

In Fig. 7c, we have plotted the distribution of particle types that do not exhibit pristine crystalline habits but rather are recognizable by their images as being either aggregate snowflakes or nearly round particles. The latter are undoubtedly raindrops at flight-level temperatures > 0°C, where their concentration increased abruptly. Above the melting level, the nearly round particles were either aggregates that produced a nearly round image, or they were rimed particles, possibly graupel. Since the liquid water content observed on these flights was generally negligible (section 2b), it is unlikely that riming could have been active enough to produce graupel in the stratiform clouds. However,

TABLE 1. Hydrometeors of various types detected by Particle Measuring Systems (PMS) probes aboard the NOAA WP3D aircraft during Summer MONEX flights into the Bay of Bengal depression of 3–8 July 1979. The data are grouped according to flight-level temperature. The total number of minutes of flight in each temperature range are indicated in parentheses. The numbers shown for each type of particle have units of number per minute. They are the average numbers of particles encountered per minute of in-cloud flight at the indicated temperature range; that is, for each type of particle, the numbers shown below are A/B, where A is the total number of particles of a given type detected while flying at levels characterized by a given temperature range, and B is the total number of minutes of flight in cloud in that temperature range. The aggregates and large dendritic crystals were identified in data from the PMS precipitation probe. All the other particle types were identified in data from the PMS cloud probe. The particle frequencies can be converted approximately to concentrations (number per liter) by dividing by the rate of air flow through the PMS probes. For the cloud probe the flow was about 22 L min^{-1}, and for the precipitation probe 283 L min^{-1}.

	Small				Large		
Temperature	Nearly round	Columns	Dendritic crystals	Needles	Plates	Aggregates	Dendritic crystals
−20.1° to −24.0°C (48 min)	1.0	0.4	0.1	0	0	0	0
−16.1° to −20.0°C (117 min)	0.6	4.3	0.6	0.1	0.1	0.5	0.02
−12.1° to −16.0°C (97 min)	0.7	3.4	0.7	0.1	0.1	6.6	0.8
−10.1° to −12.0°C (68 min)	0.9	2.0	1.5	0.3	0.2	11.7	2.3
−4.1° to −10.0°C (65 min)	1.4	1.3	2.0	0.02	0.4	27.3	4.0
0° to −4.0°C (89 min)	3.4	3.0	0.1	8.5	0.03	21.4	0.1
≥0.1°C (43 min)	16.1	0.3	0	0.5	0	7.8	0

some of the flight tracks passed close to convective cells, and rimed particles from the cells could have been detrained into the stratiform cloud regions traversed by the aircraft.

The concentration of aggregate snowflakes exhibited a pronounced maximum at flight-level temperatures between 0° and −10°C (Fig. 7c). Significantly, this maximum is centered just below the maxima of platelike and dendritic crystals seen in Fig. 7b. As pointed out by Hobbs (1974), "ice particles which occur in clouds are very variable in character and several different mechanisms might be responsible for their adhesion following collision." One of the primary mechanisms he mentions is the entwining of the branches of dendritic crystals at and below the levels where these branched particles are formed. The location of the maximum concentration of aggregates in the Bay of Bengal depression suggests that the aggregates in this case were of the type formed by the entanglement of large dendritic crystals. This inference is supported by the tendency, noted in section 3, for large dendritic crystals to be encountered wherever aggregates occurred in profusion.

These results present a rather clear picture of stratiform precipitation mechanisms. Ice crystals were growing at temperatures corresponding to their shapes and settling downward as they grew. The downward drift of the ice particles, with terminal fallspeeds of only 1–2 m s^{-1}, could only have occurred in regions of weak upward motion, of the type associated with deep stratiform cloud. Branched crystals were apparently aggregating as they descended toward the 0°C level. Consequently, aggregates were common in a 2 km deep layer just above the melting level. Below this level, the aggregates and other ice particles abruptly melted into raindrops.

This characteristically stratiform microphysical character of the clouds associated with the mesoscale rain areas of the Bay of Bengal depression confirms that the regions of more uniform moderate rain falling outside of convective cores and lines were indeed nonconvective. This result is significant since these nonconvective portions of the mesoscale rain areas dominated the total area covered by precipitation in the depression. Any view of the clouds and precipitation in the Bay of Bengal depression as entirely convective (or entirely stratiform) must be rejected.

5. Conclusions

The radar data and hydrometeor imagery obtained aboard the NOAA P3 aircraft in the 3–8 July 1979 Bay of Bengal depression in Summer MONEX have shown that the precipitation in the disturbance was concentrated in mesoscale precipitation features rather similar to those seen in equatorial cloud clusters such as those observed in GATE (Houze and Betts, 1981) and Winter MONEX (Houze et al., 1981b; Churchill and Houze, 1984a; Houze and Churchill, 1984). These precipitation features were located northwest through southwest

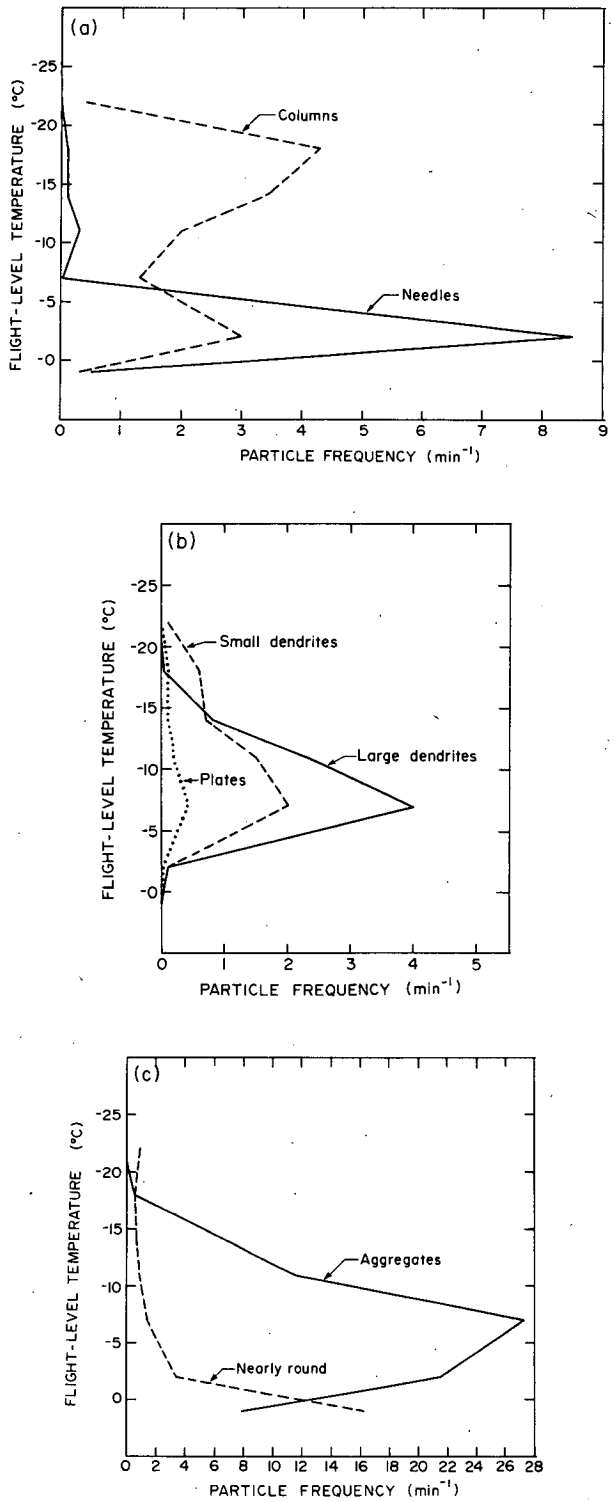

FIG. 7. Vertical distribution of hydrometeor frequencies. The number of hydrometeors of a habit observed for each minute of in-cloud flight time are plotted against the flight-level temperatures at which they were observed. Data represent the entire case study of 3, 5, 6, 7 and 8 July. (a) Columns and needles. (b) Small dendrites, large dendrites, and plates. (c) Aggregates and nearly round particles.

through southeast of the storm center and were typically 100–500 km in horizontal dimension. The larger features tended to be elongated in the east–west or northwest–southeast direction, and each mesoscale precipitation feature was characterized by a widespread cloud shield based (as found by Warner and Grumm, 1984) at about the 400 mb level. The rain falling from the cloud deck was partly convective and partly stratiform. Some of the convective towers were very intense and overshot the top of the cloud shield. However, the area covered by precipitation was dominated by the relatively uniform stratiform rain. The quantitative reliability of the P3 lower fuselage radar was not considered sufficient to make quantitative rain estimates for this depression; however, the intensities and sizes of the convective and stratiform echoes in this storm appeared rather similar to those seen in GATE and Winter MONEX cloud clusters, in which some 30%–50% of the total precipitation was found to be stratiform (Houze and Hobbs, 1982; Leary, 1984).

In some of the mesoscale precipitation features in the Bay of Bengal depression, the convective portion of the rain area consisted of intense cores arranged spatially within the stratiform region in no readily identifiable pattern. These mesoscale precipitation features may be analogous to the "nonsquall" cloud clusters identified in GATE (Houze and Betts, 1981). In other mesoscale features in the depression, the convective region consisted of an arc-shaped, southward-moving line of intense convective rain oriented generally east–west and followed (to the north) by a wide region of stratiform cloud and precipitation. The orientation and structure of the arc lines may have been related to the strong easterly monsoonal shear in this region. These arc-line mesoscale precipitation features in the depression may be analogous to the "squall" clusters identified in GATE by Houze and Betts (1981).

The stratiform regions of the mesoscale precipitation features in the depression were traversed extensively by the P3 aircraft at flight levels ranging from +5° to −25°C in temperature. The hydrometeor images obtained on these flights provided a unique view of the precipitation mechanisms at work in the stratiform regions of the mesoscale precipitation features. Liquid water was virtually absent above the 0°C level. Ice particle shapes were distributed in the vertical in accordance with a picture of crystals growing in habits determined by the ambient temperature and then drifting downward. Pristine shapes, including needles, columns, plates and branched crystals were all seen in maximum concentration at flight levels about 1 km below the altitude at which their growth habit was determined. Large dendritic crystals were apparently aggregating to form large snowflakes as they fell from the −17°C level toward the melting level. As ice particles fell below the melting level, they abruptly melted into raindrops.

This consistent picture of stratiform precipitation

growth and fallout prevailed along 50–300 km segments of flight tracks. This result implies that updrafts strong enough to promote ice particle growth, but not strong enough to prevent sedimentation of the particles or to maintain liquid water in the presence of the ice, must have prevailed above the 0°C level throughout the stratiform regions of the mesoscale precipitation features in the Bay of Bengal depression.

The radar and cloud microphysical observations obtained in the Bay of Bengal depression thus indicate that vertical air motions that produced the precipitation in this storm were partly contained within deep convective cores and partly in gentler but broader mesoscale updrafts, which promoted stratiform precipitation. In this respect, the mesoscale precipitation features of the Bay of Bengal depression closely resembled the equatorial cloud clusters observed in GATE and Winter MONEX. Apparently, large-scale ascent associated with the depression (Sanders, 1984) triggered mesoscale cloud features similar to cloud clusters. As in the case of cloud clusters, the vertical distribution of latent heat release was likely quite different in the convective and stratiform portions of the mesoscale cloud features (Houze, 1982). It seems likely that these vertical distributions of heating are important to the dynamics of the depression and that parameterizations of the cloud and precipitation processes in the depression that are formulated on the premise that all of the precipitation occurs in an ensemble of purely convective towers (Krishnamurti et al., 1976; Shukla, 1978) do not contain all of the salient physics. The stratiform as well as the convective structure of the precipitating clouds will have to be accounted for in any complete future understanding of the dynamics of this type of storm.

Acknowledgments. Dr. Paul Herzegh was the radar and cloud-physics scientist on board the NOAA WP3D aircraft, and he processed the PMS particle images for us. Abhik Biswas and Terri Rottman reduced the microphysical data, and Kay Moore drafted the figures. This research was sponsored by the National Science Foundation, Grant ATM-8413546, and the Scientific Computing Division of the National Center for Atmospheric Research.

REFERENCES

Cannon, T. W., 1976: Imaging devices. *Atmos. Technol.*, **8,** 32–37.

Churchill, D. D., and R. A. Houze, Jr., 1984a: Development and structure of winter monsoon cloud clusters on 10 December 1978. *J. Atmos. Sci.*, **41,** 933–960.

——, and ——, 1984b: Mesoscale updraft magnitude and cloud-ice content deduced from the ice budget of a tropical cloud cluster. *J. Atmos. Sci.*, **41,** 1717–1725.

Gamache, J. F., and R. A. Houze, Jr., 1982: Mesoscale air motions associated with a tropical squall line. *Mon. Wea. Rev.*, **110,** 118–135.

Godbole, R. V., 1977: The composite structure of the monsoon depression. *Tellus,* **29,** 25–40.

Heymsfield, A. J., 1976: Particle size distribution measurement: An evaluation of the Knollenberg optical array probes. *Atmos. Technol.*, **8,** 17–24.

Hobbs, P. V., 1974: *Ice Physics.* Clarendon Press, 803 pp.

Houze, R. A., Jr., 1977: Structure and dynamics of a tropical squall-line system. *Mon. Wea. Rev.*, **105,** 1540–1567.

——, 1982: Cloud clusters and large-scale vertical motions in the tropics. *J. Meteor. Soc. Japan,* **60,** 396–410.

——, and A. K. Betts, 1981: Convection in GATE. *Rev. Geophys. Space Phys.*, **19,** 541–576.

——, and P. V. Hobbs, 1982: Organization and structure of precipitating cloud systems. *Advances in Geophysics,* **24,** 225–315.

——, and D. D. Churchill, 1984: Microphysical structure of winter monsoon cloud clusters. *J. Atmos. Sci.*, **41,** 3405–3411.

——, S. G. Geotis, F. D. Marks, Jr., D. D. Churchill and P. H. Herzegh, 1981a: Comparison of airborne and land-based radar measurements of precipitation during Winter MONEX. *J. Appl. Meteor.*, **20,** 772–783.

——, S. G. Geotis, F. D. Marks, Jr. and A. K. West, 1981b: Winter monsoon convection in the vicinity of north Borneo. Part I: Structure and time variation of the clouds and precipitation. *Mon. Wea. Rev.*, **109,** 1595–1614.

Johnson, R. H., and R. A. Houze, Jr., 1987: Precipitating cloud systems of the Asian monsoon. *Reviews in Monsoon Meteorology,* C.-P. Chang and T. N. Krishnamurti, Eds., in press.

Knollenberg, R. G., 1970: The optical array: An alternative to scattering or extinction for airborne particle size determination. *J. Appl. Meteor.*, **9,** 86–103.

Krishnamurti, T. N., M. Kanamitsu, R. Godbole, C. B. Chang, F. Carr and J. H. Chao, 1976: Study of a monsoon depression (II), dynamical structure. *J. Meteor. Soc. Japan,* **54,** 208–225.

——, Y. Ramanathan, P. Ardanoy, R. Pasch and P. Greiman, 1980: *Quick Look 'Summer MONEX Atlas' Part III: Monsoon Depression Phase,* FSU Rep. No. 80-8. Department of Meteorology, Florida State University, Tallahassee, Florida, 32306. 135 pp.

Leary, C. A., 1984: Precipitation structure of the cloud clusters in a tropical easterly wave. *Mon. Wea. Rev.*, **112,** 313–325.

Nitta, T., and K. Masuda, 1981: Observational study of a monsoon depression developed over the Bay of Bengal during Summer MONEX. *J. Meteor. Soc. Japan,* **59,** 672–681.

Ramage, C. S., 1971: *Monsoon Meteorology.* Academic Press, 271 pp.

Rao, Y. P., 1976: *Southwest Monsoon.* Meteor. Monogr. Synoptic Meteorology No. 1/1976. Indian Department of Meteorology, New Delhi, 367 pp.

Sanders, F., 1984: Quasi-geostrophic diagnosis of the monsoon depression of 5–8 July 1979. *J. Atmos. Sci.*, **41,** 538–552.

Shukla, J., 1978: CISK-barotropic-baroclinic instability and the growth of monsoon depressions. *J. Atmos. Sci.*, **35,** 495–508.

Wallace, J. M., and P. V. Hobbs, 1977: *Atmospheric Science: An Introductory Survey.* Academic Press, 467 pp.

Warner, C., 1982: Mesoscale features and cloud organization on 10–12 December 1978 over the South China Sea. *J. Atmos. Sci.*, **39,** 1619–1641.

——, 1984a: Core structure of a Bay of Bengal monsoon depression. *Mon. Wea. Rev.*, **112,** 137–152.

——, 1984b: Satellite Observations of a Monsoon Depression. Department of Environmental Sciences, Clark Hall; University of Virginia; Charlottesville, VA 22903. Final report to NASA under Grant NAG 5-297. 54 pp.

——, and R. H. Grumm, 1984: Cloud distributions in a Bay of Bengal monsoon depression. *Mon. Wea. Rev.*, **112,** 153–172.

Zipser, E. J., 1969: The role of organized unsaturated convective downdrafts in the structure and rapid decay of an equatorial disturbance. *J. Appl. Meteor.*, **8,** 799–814.

——, 1977: Mesoscale and convective-scale downdrafts as distinct components of squall-line circulation. *Mon. Wea. Rev.*, **105,** 1568–1589.